NASA TECHNICAL REPORT

NASA TR R-221

NASA TR R-221

ANALYSIS OF HYPERVELOCITY PERFORMATION OF A VISCO-PLASTIC SOLID INCLUDING THE EFFECTS OF TARGET-MATERIAL YIELD STRENGTH

by Robert G. Thomson

Langley Research Center
Langley Station, Hampton, Va.

NATIONAL AERONAUTICS AND SPACE ADMINISTRATION • WASHINGTON, D. C. • APRIL 1965

DISCLAIMER NOTICE

THIS DOCUMENT IS BEST QUALITY AVAILABLE. THE COPY FURNISHED TO DTIC CONTAINED A SIGNIFICANT NUMBER OF PAGES WHICH DO NOT REPRODUCE LEGIBLY.

NASA TR R-221

ANALYSIS OF HYPERVELOCITY PERFORATION OF A VISCO-PLASTIC SOLID INCLUDING THE EFFECTS OF TARGET-MATERIAL YIELD STRENGTH

By Robert G. Thomson

Langley Research Center
Langley Station, Hampton, Va.

NATIONAL AERONAUTICS AND SPACE ADMINISTRATION

For sale by the Office of Technical Services, Department of Commerce,
Washington, D.C. 20230 -- Price $2.00

ANALYSIS OF HYPERVELOCITY PERFORATION OF A VISCO-PLASTIC SOLID INCLUDING THE EFFECTS OF TARGET-MATERIAL YIELD STRENGTH

By Robert G. Thomson
Langley Research Center

SUMMARY

A visco-plastic flow theory for the solution of hypervelocity perforation of thin plates has been investigated. A short-time analytical solution of the governing equation including the effects of yield strength of the target material was obtained and expressions were derived for the velocities, displacements, strains, and strain rates present in the target material during hypervelocity impact. In addition, pertinent parameters have been varied and a comparison has been made with the solution in which the yield strength was neglected. The results indicate that the velocities, displacements, and stresses determined from the present solution are at times markedly different from the results obtained when the yield strength is neglected. The effects on the radius of perforation of the plate material when the yield strength is included were found to be not as significant as those of the solution neglecting target yield strength and resulted in little variation in the computed perforation radii.

INTRODUCTION

A visco-plastic flow theory was first proposed for the hypervelocity perforation of thin plates by rigid cylindrical projectiles by F. A. Bakhshiyan in 1948. (See ref. 1.) In this analysis a circular cylindrical projectile was considered to impact upon a thin target plate and the resulting radial visco-plastic boundary was treated as time dependent. The solution presented, however, was limited to the special case of an infinite mass projectile. In references 2 and 3 an analytical solution was obtained for a problem similar to that of reference 1 except that the yield strength of the target plate was taken to be zero (that is, the visco-plastic boundary was taken to be at infinity) and the projectile mass was treated as finite. The yield strength of the target material was introduced later in this analysis to establish a separation criterion for perforation. An approximate two-dimensional analysis of the impact problem as stated in reference 2 is presented in reference 4. This solution indicates that the radial velocities are about one order of magnitude less than the axial velocities and thus helps to justify the use of a one-dimensional approach.

An extension of the work presented in references 2 and 3 is presented in reference 5 in which an attempt is made to include the effects of target material yield strength in the governing differential equation and associated boundary conditions. The results of the analysis are given in finite series form and a parametric study is presented in which the effects of variations in the pertinent parameters on the radius of perforation are determined. The solution as given in reference 5, however, does indicate that for the case of the infinite mass projectile, the velocity of the projectile decreases slightly after impact. This result is probably due to the fact that only a finite number of terms from an infinite series was used.

In the present analysis an analytical solution to the problem of a rigid projectile of finite mass impacting upon an infinite plate is obtained in which yield-strength considerations have been included in both the analysis and in the determination of the separation criterion. The solution obtained in the present report differs from that reported in reference 5 even though the basic problem is identical. The present solution agrees in the limiting case when the yield strength is set equal to zero with the solution presented in references 2 and 3 in which yield strength was neglected. In addition, the expression for velocity will limit, in the case of the infinite mass projectile, to the condition that the velocity of the projectile remains constant after impact.

The present report also shows how the effects of including yield strength in the analysis compare with the results obtained for the same conditions when yield strength is neglected. Some pertinent parameters such as initial velocity and mass of the impacting projectile as well as the plate thickness and viscosity are varied in order to study their effects on the displacement, velocity, strain, and strain-rate distributions, and on the radius of perforation as computed with and without target yield strength.

SYMBOLS

A,B	coefficients of Bessel functions
a	radius of projectile
C_1	dynamic ultimate yield strain in shear
erf	error function
erf'	derivative of error function
erfc	complementary error function
g_o	initial projectile velocity

h	plate thickness
$\zeta = \frac{2\pi ah}{M}$	
$H = \frac{2\pi a^2 h\rho}{M}$; also used for Hankel function	
$i^n\text{erfc } x$	nth integral of erfc x (see appendix, eq. (A38))
I_n	modified Bessel function of first kind of order n
J_n	Bessel function of first kind of order n
k	dynamic target yield stress in shear
K	Bingham number, $\frac{ka}{V_o\mu}$
K_n	modified Bessel function of second kind of order n
M_1	mass of projectile
M	mass of projectile and plug of plate material of radius a, $M_1 + \pi a^2 h\rho$
n,p	integers
r	radial distance
$\bar{r}$	nondimensional radial distance, $\frac{r}{a}$
s	Laplace transform parameter
S_p	Struve function of order p
t	time
$\bar{t}$	nondimensional time, $\frac{v}{a^2}t$
V	axial velocity
$\bar{V}$	transform of V
θ	angle in plane of target (see fig. 1)

V_o initial velocity of projectile after impact

$\frac{V}{V_o}$ nondimensional velocity

$\frac{\partial V}{\partial r}\frac{a}{V_o}$ nondimensional shear strain rate

w axial displacement

$w\frac{\nu}{a^2 V_o}$ nondimensional displacement

$\frac{\partial w}{\partial r}\frac{\nu}{aV_o}$ nondimensional shear strain

Y_n Bessel function of second kind of order n

γ shear strain, $\frac{\partial w}{\partial r}$

μ dynamic coefficient of viscosity

ν kinematic coefficient of viscosity, $\frac{\mu}{\rho}$

ρ mass density of plate material

τ_{rz} transverse shear stress

z axial coordinate

Subscripts:

cr critical

p perforation

A dot over a symbol denotes differentiation with respect to time t.

ANALYSIS

Governing Equations

In the present analysis a rigid cylindrical projectile is considered to impact upon a thin infinite plate. The resulting perforation of the plate by the projectile is assumed to be a simple shear-plugging perforation in which only the transverse shear stresses act to resist the inertia of the impacting projectile. The perforation is also considered to be axially symmetric and the

shear stress is taken to be constant through the thickness of the plate. The resulting deformations w of the plate are then represented as functions only of the radial coordinate r and the time t, both being independent of the axial coordinate z and the circumferential coordinate θ. (See fig. 1(a).) Hence, by taking the sum of the forces in the axial direction on a circular ring element of plate material (see fig. 1(b)), the basic equation of motion for this simple shear perforation model can be written as

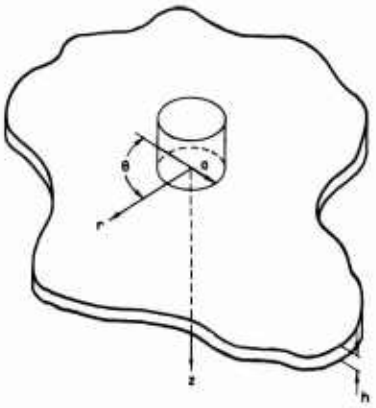

(a) Finite rigid projectile and infinite plate.

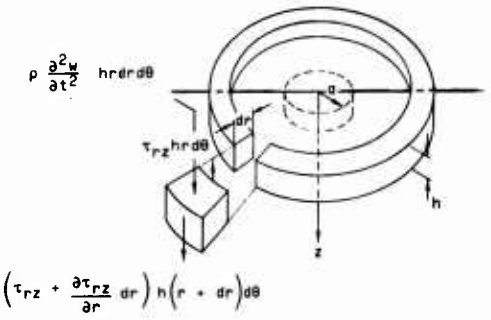

(b) Circular ring element with equilibrium forces.

Figure 1.- Geometry and coordinate system of perforation.

$$\frac{\partial \tau_{rz}}{\partial r} + \frac{\tau_{rz}}{r} = \rho \frac{\partial^2 w}{\partial t^2} \qquad (1)$$

The plate material considered herein is assumed to behave like an incompressible, visco-plastic Bingham solid in which the deformation accompanying transverse shearing commences only after the yield strength of the material has been reached. (See ref. 6.) When the value of the transverse shear stress falls below the yield stress of the material (or when the rate of deformation becomes equal to zero), visco-plastic flow ceases and the material is assumed to be rigid. The relation between the shear strain rate and shearing stress for the case of simple shear perforation can be written as (see ref. 6)

$$\tau_{rz} = \mu \frac{\partial \dot{w}}{\partial r} + \left(\text{sign } \frac{\partial \dot{w}}{\partial r}\right) k \qquad (2a)$$

or, since the sign $\frac{\partial \dot{w}}{\partial r}$ is always negative in this case,

$$\tau_{rz} = \mu \frac{\partial \dot{w}}{\partial r} - k \qquad (2b)$$

where

μ dynamic viscosity of target material

k dynamic yield stress in shear of target material

$\frac{\partial \dot{w}}{\partial r} = \frac{\partial V}{\partial r}$ = shear strain rate

and the relations between the velocity V, axial displacement w, and strain γ, are

$$V = \frac{\partial w}{\partial t}$$

$$\gamma = \frac{\partial w}{\partial r}$$

$$\frac{\partial \gamma}{\partial t} = \frac{\partial V}{\partial r}$$

Substitution of equation (2b) into equation (1) yields the governing linear differential equation

$$\frac{\partial^2 V}{\partial r^2} + \frac{1}{r}\frac{\partial V}{\partial r} - \frac{1}{\nu}\frac{\partial V}{\partial t} = \frac{1}{r}\frac{k}{\mu} \tag{3}$$

where ν is the coefficient of kinematic viscosity. The initial conditions are taken to be

$$V = 0 \qquad (t = 0,\ r > a) \tag{4}$$

$$V = V_o \qquad (t = 0,\ r \leqq a) \tag{5}$$

where V_o is the initial velocity of the projectile and plug combination. In this study V_o was determined from the conservation of momentum at the instant of impact in which the projectile-plug combination is assumed to be rigid and to act as a unit. Thus

$$V_o = g_o \frac{M_1}{M} \tag{6}$$

where

g_o initial velocity of free projectile

M_1 mass of projectile

$M = M_1 + \pi a^2 h \rho$

The boundary conditions are

$$-\zeta k + \mu\zeta\frac{\partial V}{\partial r} - \frac{\partial V}{\partial t} = 0 \qquad (t > 0,\ r = a) \tag{7}$$

and

$$V \to 0 \qquad (t \geqq 0,\ r \to \infty) \qquad (8)$$

where

$$\zeta = \frac{2\pi ah}{M}$$

Method of Solution and Resulting Equations

An analytical solution is obtained in the present paper by Laplace transform techniques similar to the approach used in reference 5. The homogeneous solution can be written directly in terms of modified Bessel functions. The particular solution, however, is obtained by utilizing Struve functions of order zero rather than by the method of variation of parameters used in reference 5. The solution to the governing differential equation (eq. (3)) and its associated boundary conditions (eqs. (4), (5), (7), and (8)) is discussed in detail in the appendix. The solutions obtained are "short time" solutions in t corresponding to values of the transform parameter $s > \frac{\nu}{a^2}$ or $t < \frac{a^2}{4\nu}$ (see appendix) resulting from the use of asymptotic expansions in the transformed state. It is shown in the appendix that the velocity (eq. (A34)), displacement (eq. (A37)), shear strain (eq. (A36)), and shear strain rate (eq. (A35)) can be expressed in dimensionless form in terms of a dimensionless radius $\bar{r}$ and a dimensionless time $\bar{t}$ as

$$\frac{V}{V_o} = \frac{1}{\sqrt{\bar{r}}}\left\{\operatorname{erfc}\frac{\bar{r}-1}{2\sqrt{\bar{t}}} + 4K(1-H)\bar{t}\,i^2\operatorname{erfc}\frac{\bar{r}-1}{2\sqrt{\bar{t}}} + 16KH\bar{t}^2 i^4\operatorname{erfc}\frac{\bar{r}-1}{2\sqrt{\bar{t}}}\right.$$

$$+ R_1\left[2\sqrt{\bar{t}}\,i\operatorname{erfc}\frac{\bar{r}-1}{2\sqrt{\bar{t}}} + 8K(1-H)(\bar{t})^{3/2} i^3\operatorname{erfc}\frac{\bar{r}-1}{2\sqrt{\bar{t}}} + 32KH(\bar{t})^{5/2} i^5\operatorname{erfc}\frac{\bar{r}-1}{2\sqrt{\bar{t}}}\right]$$

$$\left. + R_2\left[4\bar{t}\,i^2\operatorname{erfc}\frac{\bar{r}-1}{2\sqrt{\bar{t}}} + 16K(1-H)\bar{t}^2 i^4\operatorname{erfc}\frac{\bar{r}-1}{2\sqrt{\bar{t}}} + 64KH\bar{t}^3 i^6\operatorname{erfc}\frac{\bar{r}-1}{2\sqrt{\bar{t}}}\right]\cdots\right\} - \frac{K\bar{t}}{\bar{r}} \qquad \left((\bar{r}-1) \geqq 0\right) \qquad (9)$$

$$\frac{wv}{a^2 V_o} = \frac{4\bar{t}}{\sqrt{\bar{r}}}\left\{i^2\operatorname{erfc}\frac{\bar{r}-1}{2\sqrt{\bar{t}}} + 4K(1-H)\bar{t}\,i^4\operatorname{erfc}\frac{\bar{r}-1}{2\sqrt{\bar{t}}} + 16KH\bar{t}^2 i^6\operatorname{erfc}\frac{\bar{r}-1}{2\sqrt{\bar{t}}}\right.$$

$$+ R_1\left[2\sqrt{\bar{t}}\,i^3\operatorname{erfc}\frac{\bar{r}-1}{2\sqrt{\bar{t}}} + 8K(1-H)(\bar{t})^{3/2} i^5\operatorname{erfc}\frac{\bar{r}-1}{2\sqrt{\bar{t}}} + 32KH(\bar{t})^{5/2} i^7\operatorname{erfc}\frac{\bar{r}-1}{2\sqrt{\bar{t}}}\right]$$

$$\left. + R_2\left[4\bar{t}\,i^4\operatorname{erfc}\frac{\bar{r}-1}{2\sqrt{\bar{t}}} + 16K(1-H)\bar{t}^2 i^6\operatorname{erfc}\frac{\bar{r}-1}{2\sqrt{\bar{t}}} + 64KH\bar{t}^3 i^8\operatorname{erfc}\frac{\bar{r}-1}{2\sqrt{\bar{t}}}\right]\cdots\right\} - \frac{K\bar{t}^2}{2\bar{r}} \qquad \left((\bar{r}-1) \geqq 0\right) \qquad (10)$$

$$\frac{\partial w}{\partial r}\frac{\nu}{aV_o} = \frac{4\bar{t}}{\sqrt{\bar{r}}}\left\{-\frac{1}{2\sqrt{\bar{t}}}i^1\operatorname{erfc}\frac{\bar{r}-1}{2\sqrt{\bar{t}}} + R_3 i^2\operatorname{erfc}\frac{\bar{r}-1}{2\sqrt{\bar{t}}} + 2\sqrt{\bar{t}}\left[R_4 - K(1-H)\right]i^3\operatorname{erfc}\frac{\bar{r}-1}{2\sqrt{\bar{t}}}\right.$$

$$+ 4\bar{t}\left[R_5 + K(1-H)R_3\right]i^4\operatorname{erfc}\frac{\bar{r}-1}{2\sqrt{\bar{t}}} + 8(\bar{t})^{3/2}\left[K(1-H)R_4 - KH\right]i^5\operatorname{erfc}\frac{\bar{r}-1}{2\sqrt{\bar{t}}}$$

$$+ 16\bar{t}^2\left[KHR_3 + K(1-H)R_5\right]i^6\operatorname{erfc}\frac{\bar{r}-1}{2\sqrt{\bar{t}}} + 32(\bar{t})^{5/2}KHR_4 i^7\operatorname{erfc}\frac{\bar{r}-1}{2\sqrt{\bar{t}}}$$

$$\left. + 64\bar{t}^3 KHR_5 i^8\operatorname{erfc}\frac{\bar{r}-1}{2\sqrt{\bar{t}}} \cdots\right\} + \frac{K\bar{r}^2}{2\bar{r}^2} \qquad \left((\bar{r}-1) \geq 0\right) \qquad (11)$$

$$\frac{\partial V}{\partial r}\frac{a}{V_o} = \frac{1}{\sqrt{\bar{r}}}\left\{-\frac{1}{\sqrt{\pi\bar{t}}}e^{-\frac{(\bar{r}-1)^2}{4\bar{t}}} + R_3\operatorname{erfc}\frac{\bar{r}-1}{2\sqrt{\bar{t}}} + 2\sqrt{\bar{t}}\left[R_4 - K(1-H)\right]i\operatorname{erfc}\frac{\bar{r}-1}{2\sqrt{\bar{t}}}\right.$$

$$+ 4\bar{t}\left[R_5 + K(1-H)R_3\right]i^2\operatorname{erfc}\frac{\bar{r}-1}{2\sqrt{\bar{t}}} + 8(\bar{t})^{3/2}\left[K(1-H)R_4 - KH\right]i^3\operatorname{erfc}\frac{\bar{r}-1}{2\sqrt{\bar{t}}}$$

$$+ 16\bar{t}^2\left[KHR_3 + K(1-H)R_5\right]i^4\operatorname{erfc}\frac{\bar{r}-1}{2\sqrt{\bar{t}}} + 32(\bar{t})^{5/2}KHR_4 i^5\operatorname{erfc}\frac{\bar{r}-1}{2\sqrt{\bar{t}}}$$

$$\left. + 64\bar{t}^3 KHR_5 i^6\operatorname{erfc}\frac{\bar{r}-1}{2\sqrt{\bar{t}}} \cdots\right\} + \frac{K\bar{t}}{\bar{r}^2} \qquad \left((\bar{r}-1) \geq 0\right) \qquad (12)$$

where

$$H = \frac{2\pi a^2 h\rho}{M}$$

$$M = \pi a^2 h\rho + M_1$$

$$K = \frac{ka}{\mu V_o}$$

$$\bar{t} = \frac{\nu}{a^2}t$$

$$\bar{r} = \frac{r}{a}$$

$$R_1 = \frac{1}{8} - \frac{1}{8\bar{r}} - H$$

$$R_2 = \frac{9}{128\bar{r}^2} - \frac{1}{64\bar{r}} - \frac{7}{128} + H\left(\frac{1}{8\bar{r}} - \frac{5}{8}\right) + H^2$$

$$R_3 = -\frac{3}{8\bar{r}} - \frac{1}{8} + H$$

$$R_4 = \frac{15}{128\bar{r}^2} - \frac{3}{64\bar{r}} + \frac{7}{128} + \frac{H}{8}\left(\frac{3}{\bar{r}} + 5\right) - H^2$$

$$R_5 = -\frac{45}{256\bar{r}^3} + \frac{3}{128\bar{r}^2} + \frac{7}{256\bar{r}} + \frac{H}{16}\left(\frac{5}{\bar{r}} - \frac{3}{\bar{r}^2}\right) - \frac{H^2}{2\bar{r}}$$

and $i^n\text{erfc}\,\frac{\bar{r}-1}{2\sqrt{\bar{t}}}$ is the nth integral of $\text{erfc}\,\frac{\bar{r}-1}{2\sqrt{\bar{t}}}$. (See eq. (A38).)

It can be seen from these equations that if the yield strength k is neglected, that is, if $K = 0$, the expressions for velocity, displacement, shear strain, and shear strain rate reduce to expressions identical to those presented in reference 3. Also in the case of the infinite mass projectile in which $H = 0$ (for $M_1 = \infty$), the expression given in equation (9) for velocity is shown to reduce to $V = V_o$ at $\bar{r} = 1$ for all values of $\bar{t}$.

Typical examples of the radial distributions of strain and strain rate as expressed in equations (11) and (12) are shown in figures 2 and 3. Typical velocity and displacement distributions as given by equations (9) and (10) are plotted in subsequent figures (figs. 9 and 10).

Separation Criteria

In order to determine the radius of the plug of plate material which is sheared (or perforated) from the plate upon impact, separation criteria were established. The criteria are based on the assumption that separation of the projectile and plug of plate material from the plate occurs when the plate material can no longer transmit shear stress. If the plate material is considered viscous, it can transmit high shear stress even though visco-plastic flow is occurring. This condition of high shear stress and visco-plastic flow exists immediately after impact when the strain rate is at a maximum and the viscous stress $\mu\frac{\partial \dot{w}}{\partial r}$ is much greater than the yield stress k of the material. (See eq. (2b).) The plate material is considered to be highly viscous when the strain rate is greater than k/μ but is considered susceptible to separation once the strain rate falls below k/μ. In other words, the strain-rate

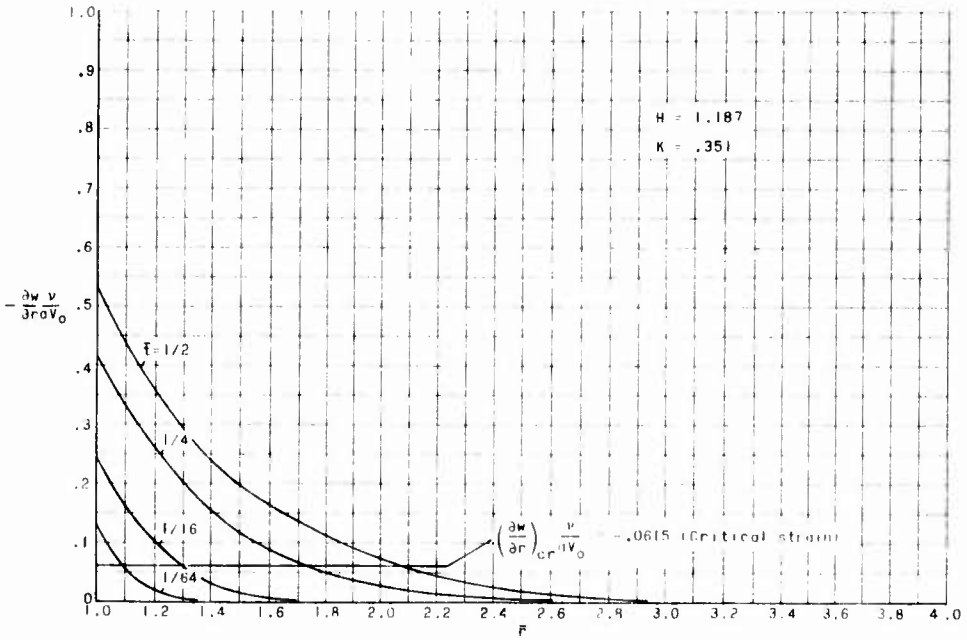

Figure 2.- Strain as a function of radius for h = 0.25 inch (0.635 cm); $M_1 = 3.56 \times 10^{-6}$ slug (51.95 mg); $\mu = 100 \frac{\text{slug}}{\text{ft-sec}} \left(0.4788 \frac{\text{Ns}}{\text{cm}^2}\right)$; g_o = 3,940 fps $\left(1{,}201 \frac{\text{m}}{\text{s}}\right)$; $\rho = 5.2 \frac{\text{slug}}{\text{ft}^3} \left(2.68 \frac{\text{g}}{\text{cm}^3}\right)$; k = 100,000 psi $\left(68.95 \frac{\text{kN}}{\text{cm}^2}\right)$; a = 0.04688 inch (0.119 cm).

criterion for separation is assumed to be

$$\left(\frac{\partial \dot{w}}{\partial r}\right)_{cr} = \frac{k}{\mu} \tag{13}$$

A second criterion deals with the shear strain of the material which at the moment of impact is zero and increases thereafter. In order for the plug to separate from the plate, the material not only has to be considered as having a sufficiently small strain rate $\left(\frac{\partial \dot{w}}{\partial r} < \frac{k}{\mu}\right)$ but also must contain large shear strains as well. The material is assumed to contain large shear strains when the shear strain exceeds a certain magnitude. The magnitude chosen in this case is the dynamic value of the ultimate shear strain of the material. Thus, the second criterion can be written as

$$\gamma_{cr} = \left(\frac{\partial w}{\partial r}\right)_{cr} = C_1 \tag{14}$$

where C_1 is the dynamic ultimate strain in shear. (A value of C_1 of 0.02 was assumed in this paper for both aluminum and steel.) For a further discussion of these separation conditions, see references 2 and 3.

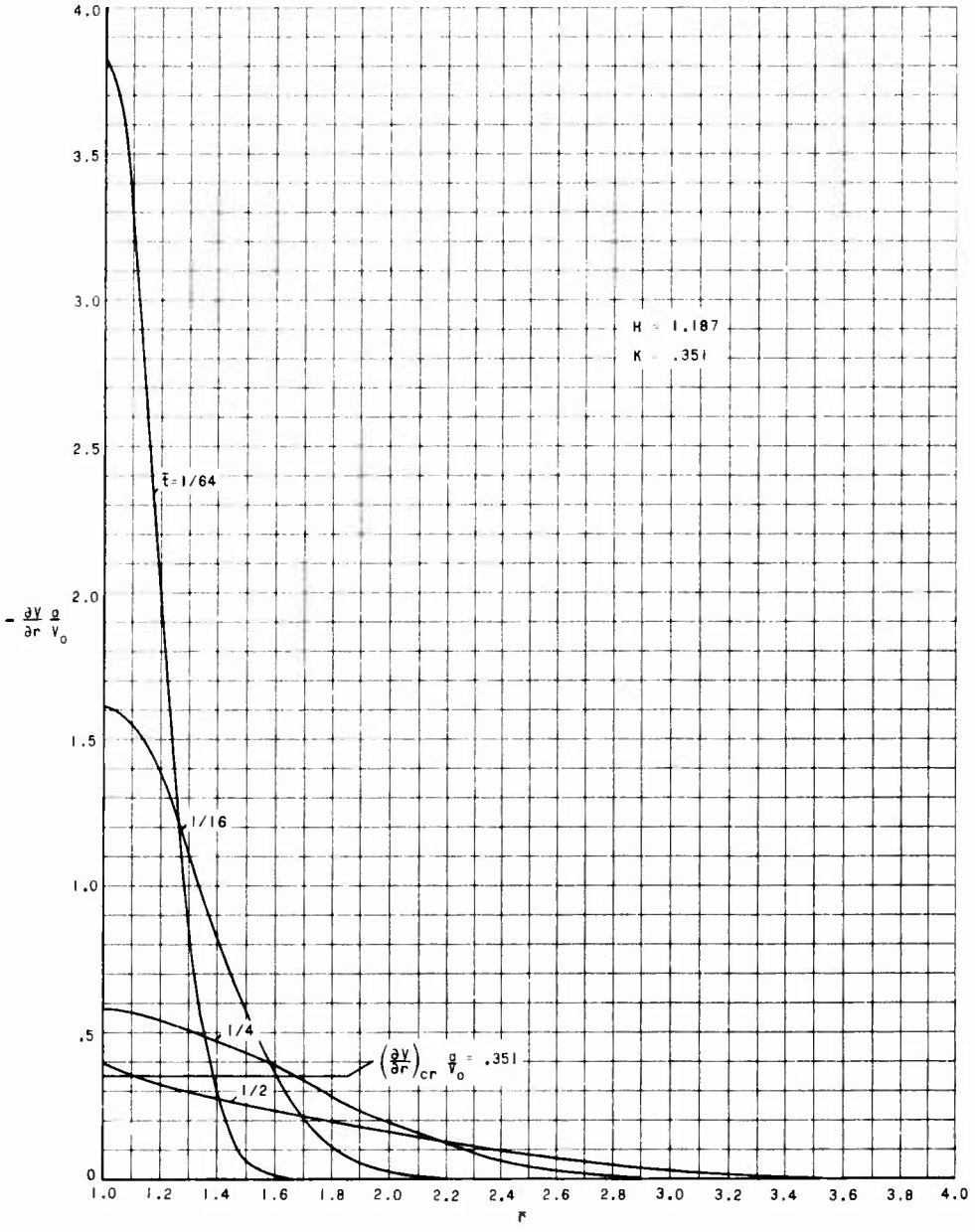

Figure 3.- Strain rate as a function of radius for h = 0.25 inch (0.635 cm); $M_1 = 3.56 \times 10^{-6}$ slug (51.95 mg); $\mu = 100 \frac{\text{slug}}{\text{ft-sec}}$ $\left(0.4788 \frac{\text{Ns}}{\text{cm}^2}\right)$; $g_o = 3{,}940$ fps $\left(1{,}201 \frac{\text{m}}{\text{s}}\right)$; $\rho = 5.2 \frac{\text{slug}}{\text{ft}^3}$ $\left(2.68 \frac{\text{g}}{\text{cm}^3}\right)$; k = 100,000 psi $\left(68.95 \frac{\text{kN}}{\text{cm}^2}\right)$; a = 0.04688 inch (0.119 cm).

The radius of separation of the plug material and the time of separation can most readily be determined by a graphical procedure. In figure 2 is shown a typical nondimensional set of curves of strain as a function of radius and in figure 3 of strain rate as a function of radius for a projectile of mass 3.56×10^{-6} slug (51.95 mg) and initial velocity 3,940 fps (1,201 m/s) impacting on a 1/4 inch (0.635 cm) thick aluminum plate. (Conversion factors for the units used herein are given in table I.) A plot of the time parameter $\bar{t}$ as a

function of $\bar{r}$ can now be obtained for critical strain from figure 2 by constructing a horizontal line representing the critical strain (eq. (14)) and determining the intersections with the strain curves. In a similar manner the critical strain-rate curve of $\bar{t}$ as a function of $\bar{r}$ can be determined from figure 3. The radius of perforation and the time of separation are then determined from the intersection of the critical strain and critical strain-rate curves as plotted in figure 4. Thus, for this particular case the radius of perforation and the time of separation are $\bar{r}_p = 1.740$ and $\bar{t} = 0.250$, respectively.

TABLE I.- CONVERSION FACTORS FOR UNITS

Parameter	U.S. Customary Unit	SI system	Conversion factor (*)
Mass	slug	milligram	14.6×10^6
Velocity	fps	$\frac{\text{meters}}{\text{second}}$	0.3048
Length	inch	centimeter	2.54
Coefficient of viscosity	$\frac{\text{lb-sec}}{\text{ft}^2}$	$\frac{\text{newton-sec}}{\text{centimeter}^2}$	0.004788
Yield strength	psi	$\frac{\text{kilonewton}}{\text{centimeter}^2}$	6.895×10^{-4}
Density	$\frac{\text{slug}}{\text{ft}^3}$	$\frac{\text{grams}}{\text{centimeter}^3}$	0.51538

*Multiply value given in U.S. customary unit by conversion factor to obtain equivalent value in SI unit.

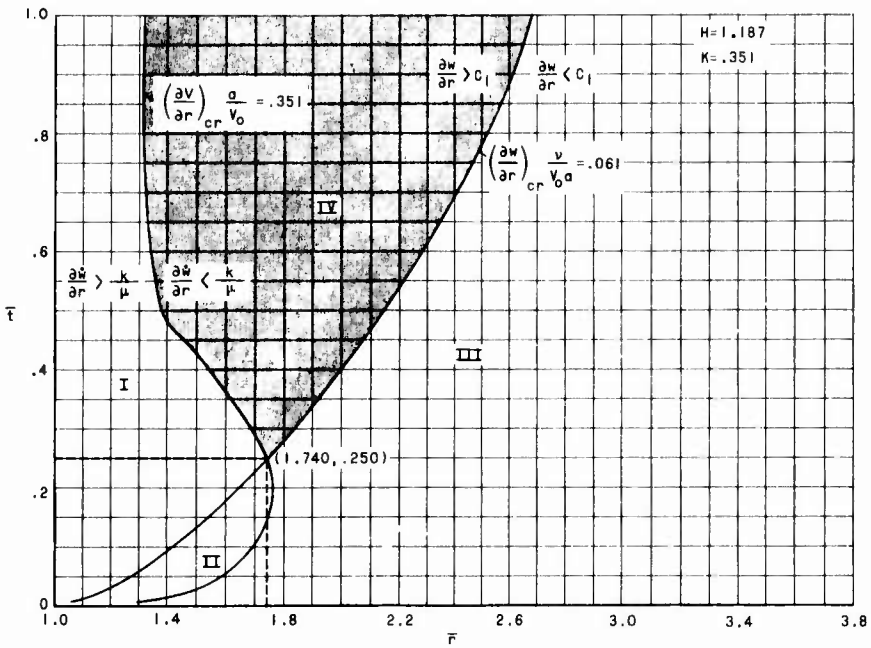

Figure 4.- Graphical representation for determining perforation radius and separation time. $h = 0.25$ inch (0.635 cm); $M_1 = 3.56 \times 10^{-6}$ slug (51.95 mg); $\mu = 100 \frac{\text{slug}}{\text{ft-sec}} \left(0.4788 \frac{\text{Ns}}{\text{cm}^2}\right)$; $g_o = 3{,}940$ fps $\left(1{,}201 \frac{\text{m}}{\text{s}}\right)$; $\rho = 5.2 \frac{\text{slug}}{\text{ft}^3} \left(2.68 \frac{\text{g}}{\text{cm}^3}\right)$; $k = 100{,}000$ psi $\left(68.95 \frac{\text{kN}}{\text{cm}^2}\right)$; $a = 0.04688$ inch (0.119 cm).

Note that four regions are indicated in figure 4. In these regions the predominant material behavior could be described as containing: large strain rates and large strain (region I); large strain rates and small strain (region II); small strain rates and small strain (region III); and small strain rates and large strain (region IV). Only in region IV are both critical components of the separation criteria satisfied; therefore, it is assumed that only in this region does separation occur.

EFFECTS OF TARGET-MATERIAL YIELD STRENGTH ON PERFORATION RADIUS

Expressions are derived in the appendix and presented in the previous section for the velocity, displacement, shear strain, and shear strain rate written in nondimensional form. These expressions contain pertinent parameters associated with the perforation problem such as projectile mass, initial velocity, target density, viscosity, yield strength, and thickness. Variations in these pertinent parameters are now investigated to determine their effects on the perforation radius. Results are obtained, with the aid of electronic computing machines, for the present solution which includes the effects of yield strength and for the simplified solution in which yield strength is neglected (that is, in which K is set equal to zero in eqs. (9), (10), (11), and (12)).

Perforation Radius as a Function of Initial Projectile Velocity

Aluminum plate.- In figure 5 is shown the variation in perforation radius with initial projectile velocity for a 1/4 inch (0.635 cm) thick aluminum plate being impacted by a 3/64 inch (0.119 cm) radius rigid cylindrical projectile. The mass of the projectile was taken to be 3.56×10^{-6} slug (51.95 mg), which for aluminum would correspond to a projectile 0.0642 inch (0.163 cm) long. The dynamic coefficient of viscosity of the plate is 100 $\frac{\text{lb-sec}}{\text{ft}^2}$ $\left(0.4788 \frac{\text{Ns}}{\text{cm}^2}\right)$ and the dynamic yield strength 100,000 psi $\left(68.95 \frac{\text{kN}}{\text{cm}^2}\right)$. As can be seen from figure 5, including material yield strength in the analysis has little effect on the perforation radius $\bar{r}_p$ for the range of velocities shown. (The maximum difference between the case $K \neq 0$ and the case $K = 0$ is of the order of 5 percent.) A calculation was made for an initial projectile velocity of 778 fps (237 m/s) and the projectile did not perforate the plate.

Steel plate.- In figure 6 is shown the variation in perforation radius with initial projectile velocity for a 0.088 inch (0.2235 cm) thick steel plate being impacted by a 3/64 inch (0.119 cm) radius rigid cylindrical projectile. The mass of the projectile was taken to be identical to the mass of the projectile impacting the aluminum target $\left(3.56 \times 10^{-6}\right.$ slug; $\left.51.95 \text{ mg}\right)$. The dynamic coefficient of viscosity of the steel plate is 300 $\frac{\text{lb-sec}}{\text{ft}^2}$ $\left(1.4364 \frac{\text{Ns}}{\text{cm}^2}\right)$ and the dynamic yield strength 200,000 psi $\left(137.9 \frac{\text{kN}}{\text{cm}^2}\right)$. Note that the weight per unit area of

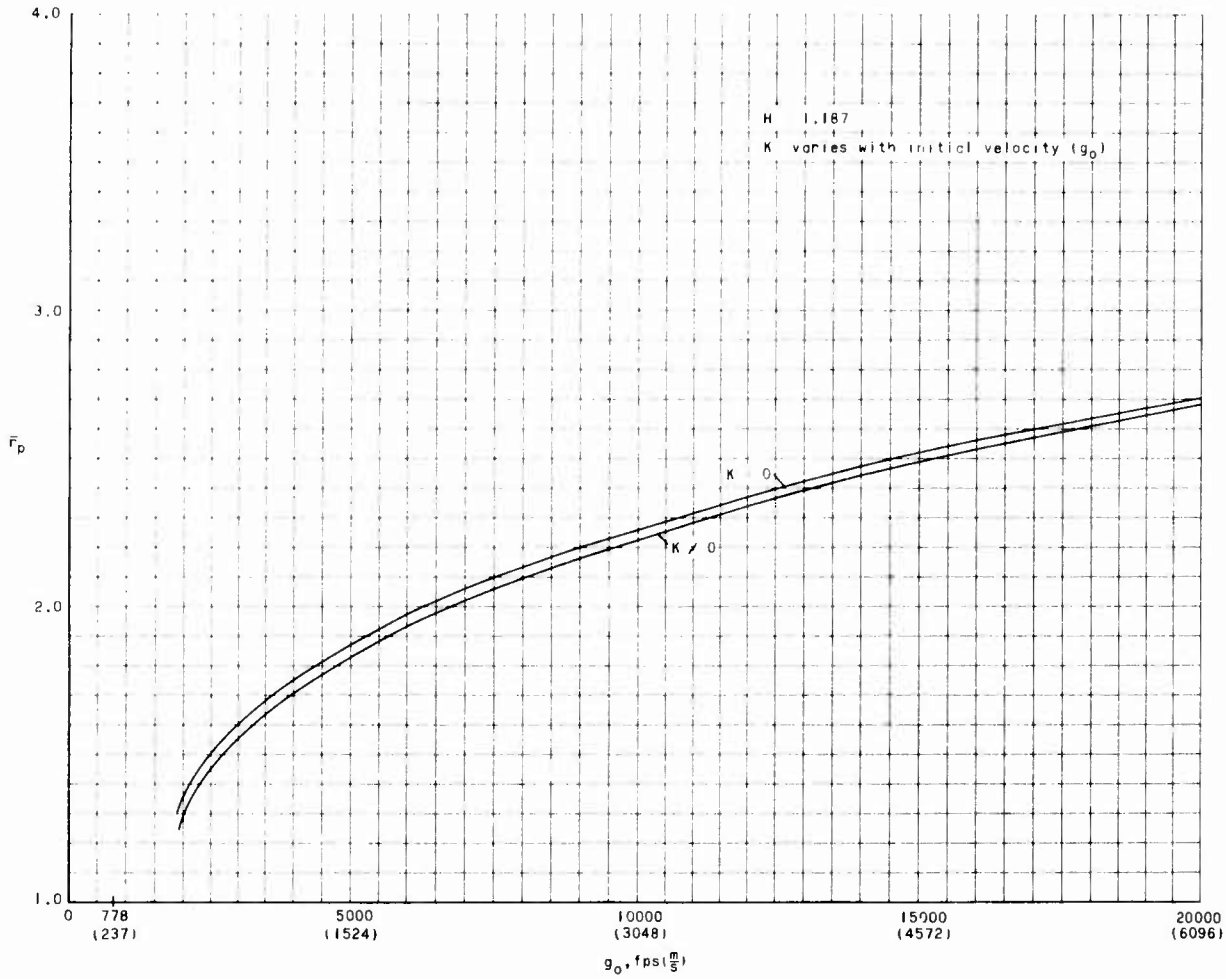

Figure 5.- Radius of perforation as a function of initial projectile velocity for aluminum plate. h = 0.25 inch (0.635 cm); $M_1 = 3.56 \times 10^{-6}$ slug (51.95 mg); $\mu = 100 \frac{\text{slug}}{\text{ft-sec}}$ $\left(0.4788 \frac{\text{Ns}}{\text{cm}^2}\right)$; $\rho = 5.2 \frac{\text{slug}}{\text{ft}^3}$ $\left(2.68 \frac{\text{g}}{\text{cm}^3}\right)$; k = 100,000 psi $\left(68.95 \frac{\text{kN}}{\text{cm}^2}\right)$; a = 0.04688 inch (0.119 cm).

the steel plate is equivalent to the weight per unit area of the aluminum plate. Thus, the momentum exchange between the impacting projectile and both the steel and aluminum plates is identical.

As can be seen from figure 6, including material yield strength in the solution still has little effect on the perforation radius over the range of velocities shown. (The maximum difference between the case $K \neq 0$ and the case $K = 0$ is of the order of 5 percent.) Although steel has a higher yield strength than aluminum, the critical strain rate, which depends on viscosity as well as yield strength, is smaller. Hence, the perforation radius in steel is larger than in aluminum (for the same initial velocities) and separation occurs after a greater passage of time. At the lower velocity range the prevention of perforation is again noted as for the aluminum target since for a specific

initial projectile velocity of 526 fps (160 m/s) the results of the analysis indicated no perforation.

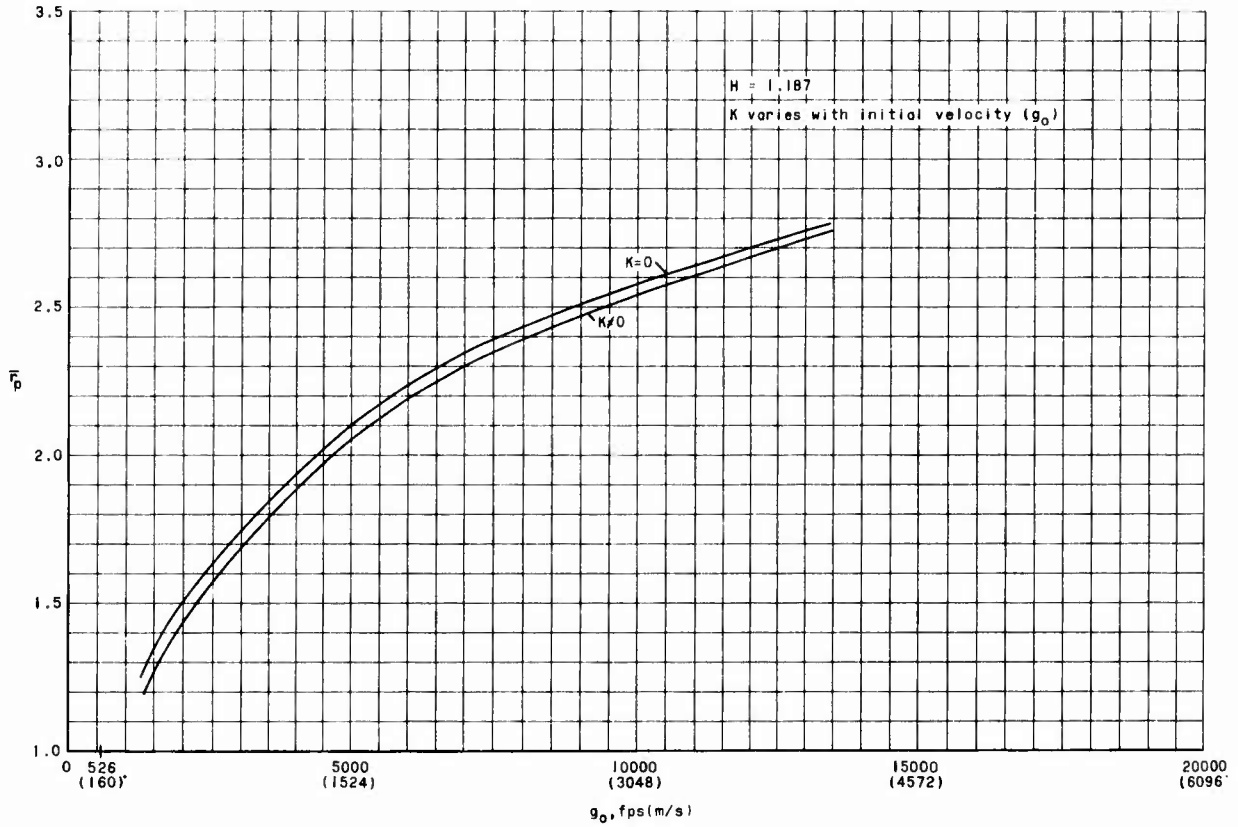

Figure 6.- Radius of perforation as a function of initial projectile velocity for steel plate. h = 0.088 inch (0.2235 cm); $M_1 = 3.56 \times 10^{-6}$ slug (51.95 mg); $\mu = 300 \frac{\text{slug}}{\text{ft-sec}}$ $\left(1.436 \frac{\text{Ns}}{\text{cm}^2}\right)$; $\rho = 14.768 \frac{\text{slug}}{\text{ft}^3}$ $\left(7.61 \frac{\text{g}}{\text{cm}^3}\right)$; k = 200,000 psi $\left(137.90 \frac{\text{kN}}{\text{cm}^2}\right)$; a = 0.04688 inch (0.119 cm).

The effect of including yield strength in the analysis when both solutions ($K = 0$ and $K \neq 0$) yield perforations has been shown to be insignificant. However, in the lower velocity ranges the simplified solution for $K = 0$ may indicate a perforation whereas the present solution for $K \neq 0$ does not. This result suggests that the present solution be applied in the case of the determination of minimum plate thicknesses necessary to prevent perforation.

Perforation Radius as a Function of Projectile Mass and/or Plate Thickness

In figure 7 is shown the effect of varying the thickness of the aluminum plate or the projectile mass on the nondimensional perforation radius. The specific initial velocity of the aluminum projectile was taken to be 20,000 fps (6,096 m/s) and the plate thickness was varied from 0.25 inch (0.635 cm) to

2.50 inch (6.35 cm), all other parameters being held constant. The increase in plate thickness decreases the perforation radius and time required for separation. Including yield strength in the analysis has little effect on the calculated perforation radii (maximum variation in calculated radii is of the order of 4 percent). Figure 7 also represents the effect of decreasing the mass of the projectile on the nondimensional perforation radius. If the mass of the aluminum projectile is decreased from 3.56×10^{-6} slug (51.95 mg) to 0.356×10^{-6} slug (5.195 mg) (the radius remaining constant) instead of the plate thickness being increased from 0.25 inch (0.635 cm) to 2.50 inch (6.35 cm), the calculated results would have identical plots. This result is due to the fact that the nondimensional parameter H $\left(\text{ratio of twice the mass of the plug directly beneath the projectile to the sum of the mass of the projectile and the mass of the self-same plug } \frac{2}{1 + \frac{M_1}{\pi a^2 \rho h}}\right)$ changes in the same proportion with a decrease in M_1 or an

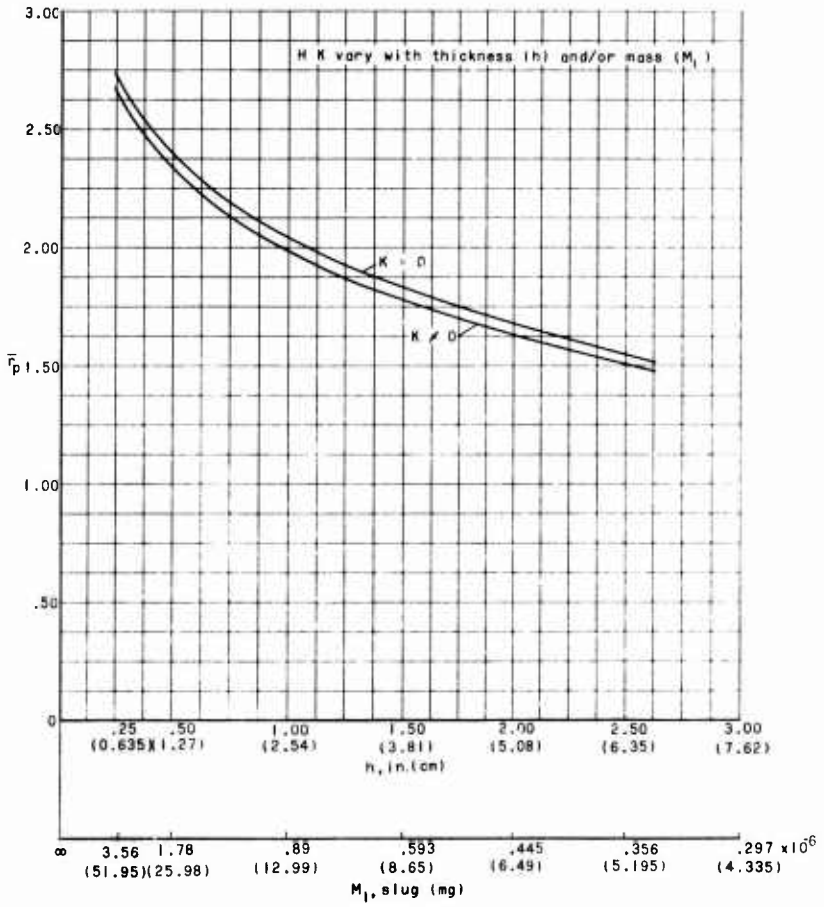

Figure 7.- Effect of variation in aluminum plate thickness and/or projectile mass on perforation radius.
$\mu = 100 \frac{\text{slug}}{\text{ft-sec}} \left(0.4788 \frac{\text{Ns}}{\text{cm}^2}\right)$; $g_o = 20{,}000$ fps $\left(6{,}096 \frac{\text{m}}{\text{sec}}\right)$;
$\rho = 5.2 \frac{\text{slug}}{\text{ft}^3} \left(2.68 \frac{\text{g}}{\text{cm}^3}\right)$; $k = 100{,}000$ psi $\left(68.95 \frac{\text{kN}}{\text{cm}^2}\right)$;
$a = 0.04688$ inch (0.119 cm).

increase in h. The perforation radius and separation time are thus seen to decrease with decreasing projectile mass. It is evident from figure 7 that the effects of yield strength need not be considered in the calculation of perforation radii.

Perforation Radius as a Function of Coefficient of Dynamic Viscosity

The variation in nondimensional perforation radii due to changes in the dynamic coefficient of viscosity is shown in figure 8 for the 3.56×10^{-6} slug (51.95 mg) projectile impacting on the aluminum plate. A specific velocity of 3,940 fps (1,201 m/s) was chosen and the dynamic coefficient of viscosity was

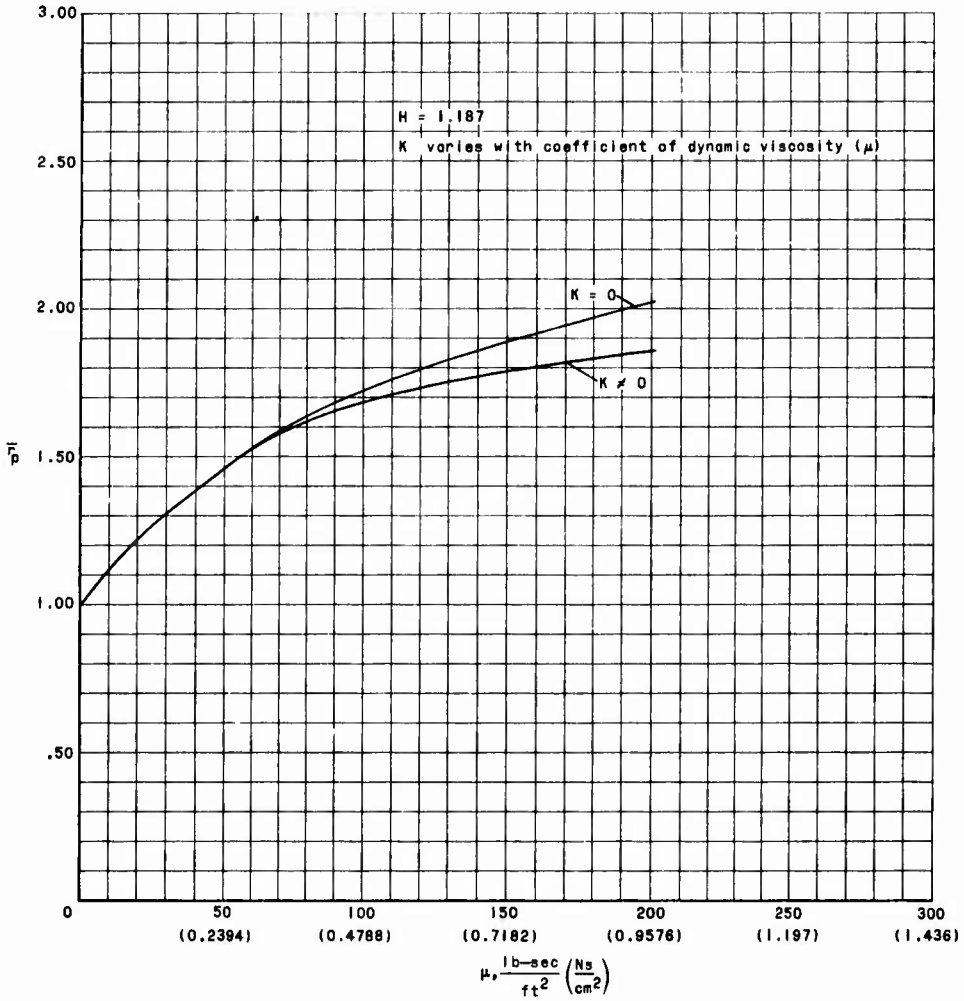

Figure 8.- Effect of variation in coefficient of dynamic viscosity on perforation radius. h = 0.25 inch (0.635 cm); $M_1 = 3.56 \times 10^{-6}$ slug (51.95 mg); g_o = 3,940 fps $\left(1{,}201 \frac{m}{s}\right)$; $\rho = 5.2 \frac{slug}{ft^3} \left(2.68 \frac{g}{cm^3}\right)$; k = 100,000 psi $\left(68.95 \frac{kN}{cm^2}\right)$; a = 0.04688 inch (0.119 cm).

varied from 0 to 200 $\frac{\text{lb-sec}}{\text{ft}^2}$ $\left(0.958 \frac{\text{Ns}}{\text{cm}^2}\right)$; all other parameters remained constant and are given in figure 8. Although calculations were made for larger values of μ, it was found that the dimensionless separation times were continuing to increase above $\bar{t} = 1/2$; and thus these results were not considered valid because of the "short time" nature of the solution. (See appendix.)

The variation in the coefficient of viscosity is shown to produce a very large variation in perforation radii and indicates a definite need for better evaluation of this coefficient. The inclusion of the yield strength in the analysis exhibits results for perforation radii as much as 10 percent lower than the solution neglecting yield strength. However, this variation can be considered to be negligible in comparison with the variations of $\bar{r}_p$ because of the lack of accurate knowledge of the coefficient of viscosity (in the present state of the art) at these high impact velocities.

EFFECTS OF TARGET-MATERIAL YIELD STRENGTH ON VELOCITIES, DISPLACEMENTS, AND STRESSES

In the previous sections it has been shown that the results for perforation radii obtained with the inclusion of yield strength in the analysis differed little from the results obtained when the yield strength was neglected. The calculations of the strain and strain rates are little affected by the inclusion of yield-strength terms and result in similar curves when plotted as a function of plate radii. The velocities, displacements, and stresses of the solution containing yield strength, however, are at times markedly different from the solution in which yield strength is neglected.

Velocities and Displacements

In figure 9 are shown the velocities and displacements plotted as a function of the plate radius for various times after impact. The pertinent parameters of the problem are those of the aluminum plate discussed earlier and are given in figure 9. (The strain and strain-rate distributions are given in figures 2 and 3 for $K \neq C$.) The specific initial velocity of the projectile is taken to be 3,940 fps (1,201 m/s). In figures 9(a) and 9(c) the results are shown for the solution neglecting yield strength whereas figures 9(b) and 9(d) show the results obtained by including yield strength. It can be seen that the two solutions begin to differ immediately and increase in variance with increasing time. The solution neglecting yield strength possesses no rigid region since $\partial V/\partial r$ never reaches zero (except at infinity), and the material remains visco-plastic everywhere. Note also, since $\partial V/\partial r$ is never zero, τ_{rz} is always greater than the yield stress (which in this case is zero) and equation (2b) for τ_{rz} is valid everywhere. The solution including yield strength, however, develops rigid and visco-plastic regions which are time dependent. A Bingham solid becomes rigid when $\partial V/\partial r$ vanishes (see ref. 6, p. 138) and $\partial V/\partial r$ vanishes at finite distances from the point of impact when

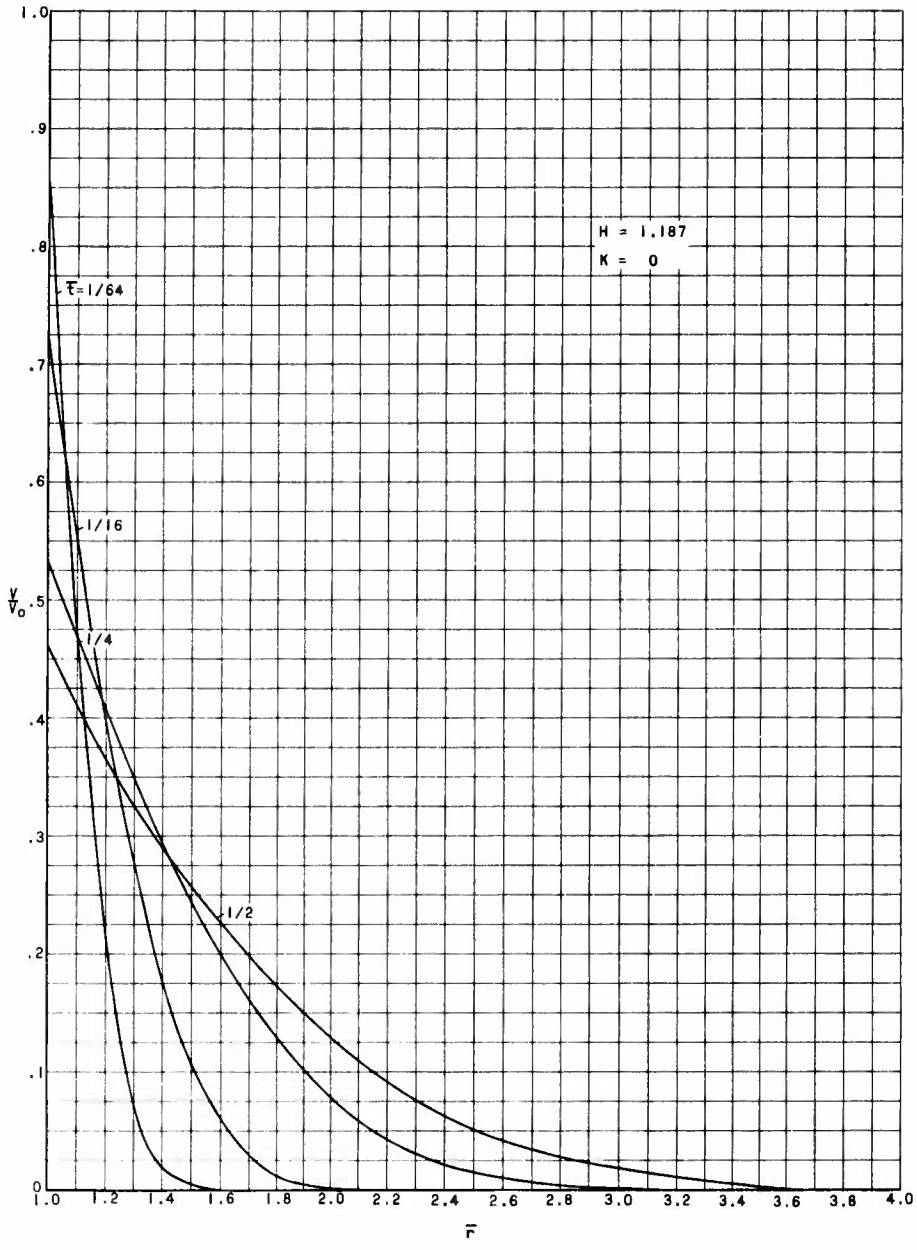

(a) Velocity as a function of radius for K = 0.

Figure 9.- Velocity and displacement as a function of radius for K = 0 and K = 0.351. h = 0.25 inch (0.635 cm); $M_1 = 3.56 \times 10^{-6}$ slug (51.95 mg); $\mu = 100 \frac{\text{slug}}{\text{ft-sec}} \left(0.4788 \frac{\text{Ns}}{\text{cm}^2}\right)$; $g_o = 3{,}940$ fps $\left(1{,}201 \frac{\text{m}}{\text{s}}\right)$; $\rho = 5.2 \frac{\text{slug}}{\text{ft}^3} \left(2.68 \frac{\text{g}}{\text{cm}^3}\right)$; k = 100,000 psi $\left(68.95 \frac{\text{kN}}{\text{cm}^2}\right)$; a = 0.04688 inch (0.119 cm).

the yield strength is included in the analysis. The second boundary condition (eq. (8)) states that as $r \to \infty$, $V \to 0$. Hence, when $\partial V/\partial r$ vanishes at a point the velocity must remain constant, and for the condition at infinity to be satisfied this constant must be zero; therefore, the rigid region possesses zero velocity. Consequently, it is concluded that when either the velocity or $\partial V/\partial r$ vanishes, the material is considered rigid.

Comparison of the velocities with and without yield strength (figs. 9(a) and 9(b)) indicates a much greater velocity decrease with time when the yield strength is included. Similarly, the displacements (figs. 9(c) and 9(d)) calculated from an analysis including yield strength are much less than those obtained when yield strength is neglected.

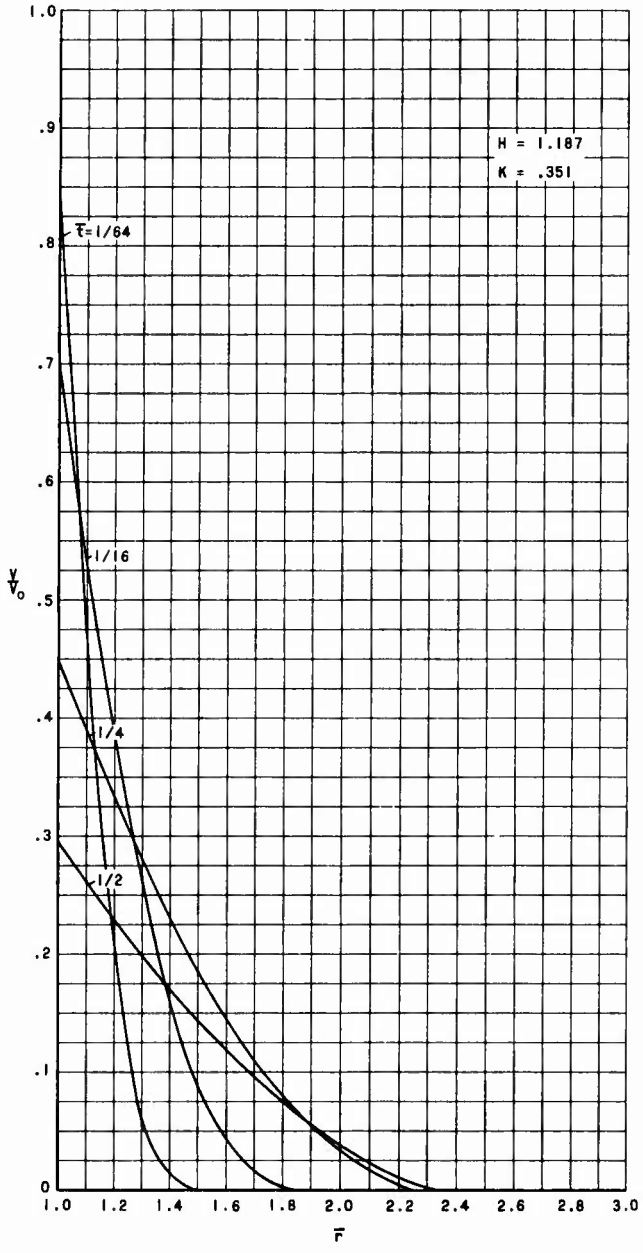

(b) Velocity as a function of radius for K = 0.351.

Figure 9.- Continued.

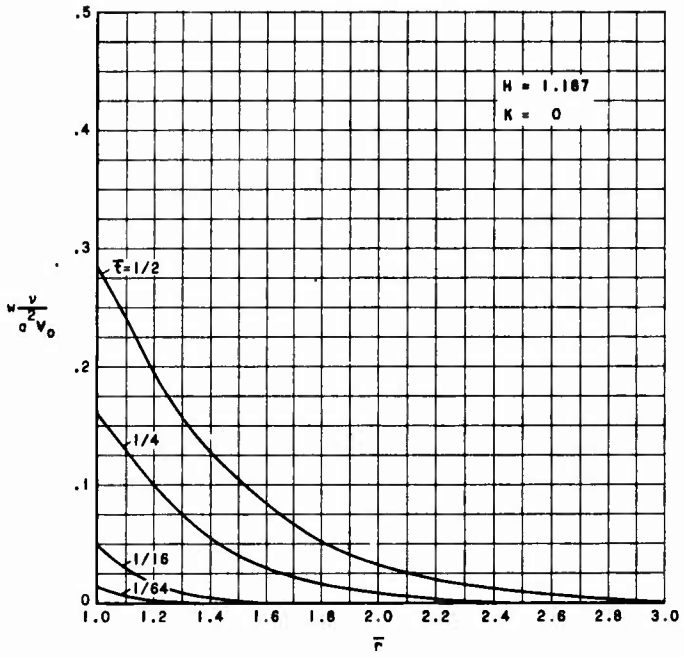

(c) Displacement as a function of radius for K = 0.

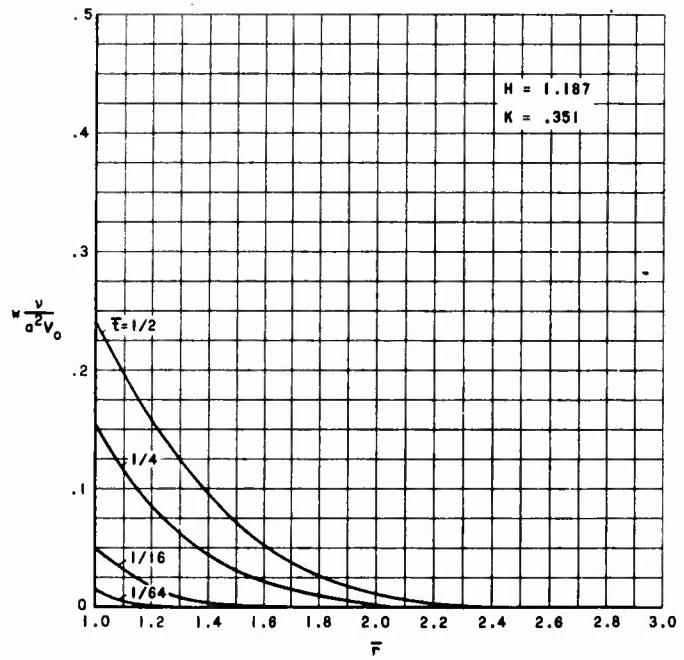

(d) Displacement as a function of radius for K = 0.351.

Figure 9.- Concluded.

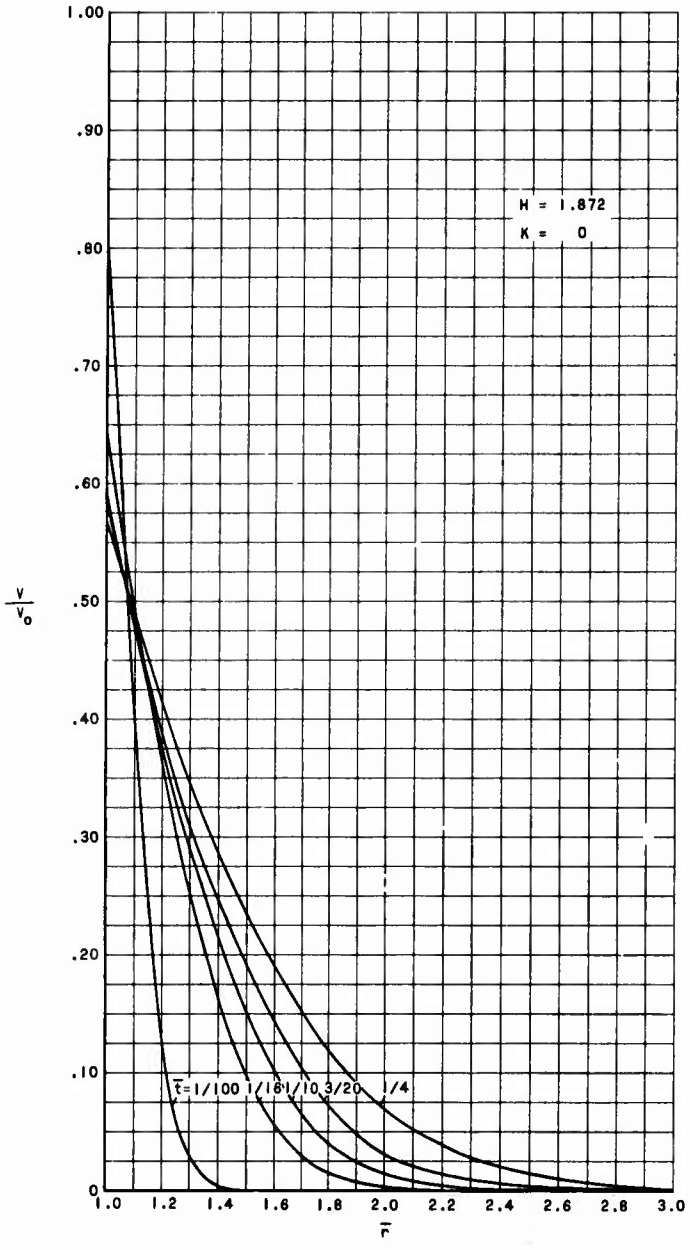

(a) Velocity as a function of radius for $K = 0$.

Figure 10.- Velocity and displacement as a function of radius for $K = 0$ and $K = 2.226$. $h = 2.5$ inch (6.35 cm); $M_1 = 3.56 \times 10^{-6}$ slug (51.95 mg); $\mu = 100 \frac{\text{slug}}{\text{ft-sec}} \left(0.4788 \frac{\text{Ns}}{\text{cm}^2}\right)$; $g_o = 3{,}940$ fps $\left(1{,}201 \frac{\text{m}}{\text{s}}\right)$; $\rho = 5.2 \frac{\text{slug}}{\text{ft}^3}$ $\left(2.68 \frac{\text{g}}{\text{cm}^3}\right)$; $k = 100{,}000$ psi $\left(68.95 \frac{\text{kN}}{\text{cm}^2}\right)$; $a = 0.04688$ inch (0.119 cm).

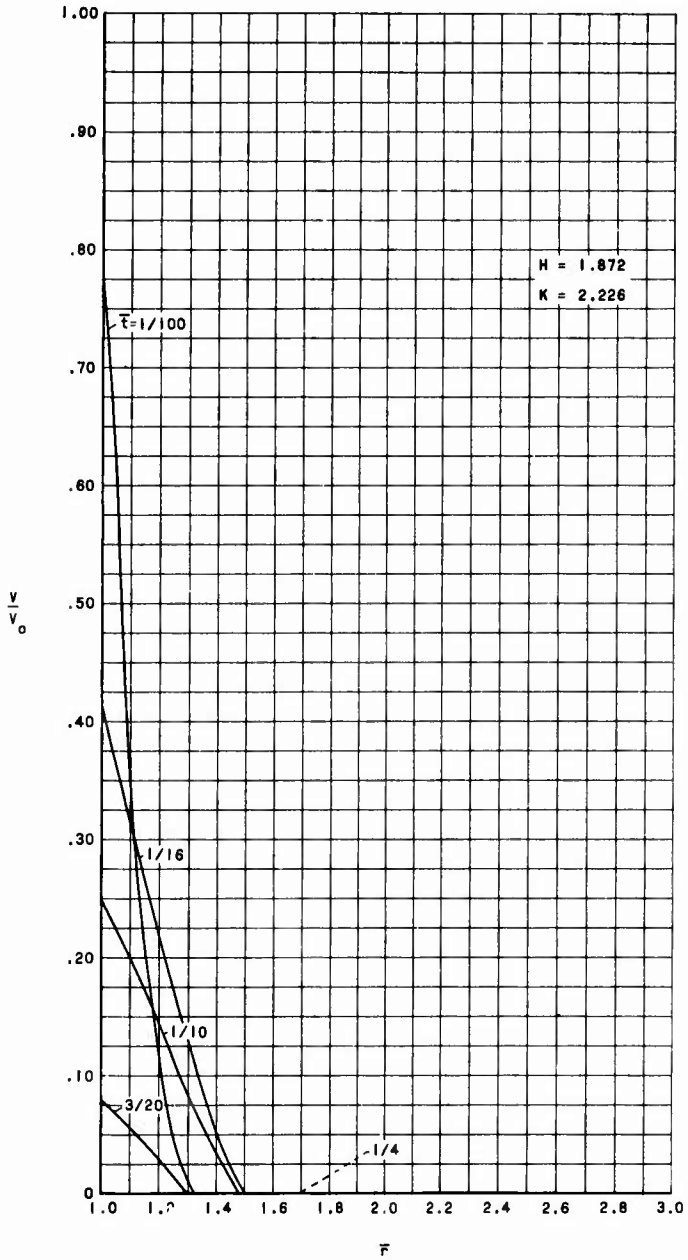

(b) Velocity as a function of radius for K = 2.226.

Figure 10.- Continued.

If the projectile mass is decreased to one-tenth its value (or the plate thickness is increased tenfold) and the perforation radius is evaluated, it is found that the projectile fails to perforate the plate. The results of such a decrease in projectile mass (or increase in plate thickness) are shown in figure 10 for the aluminum plate. Again, figures 10(a) and 10(c) show results obtained by neglecting yield strength whereas figures 10(b) and 10(d) show results obtained by including yield strength.

Note that the solution including yield strength possesses both a visco-plastic region and a rigid region, whereas for $K = 0$, the rigid region has retreated to infinity. Also note that when the yield strength is neglected, the velocity at $\bar{r} = 1$ approaches a limit as time increases but does not drop to zero. However, when the yield strength is included (see fig. 10(b)), the velocity drops to zero for all $\bar{r}$ and the material is considered rigid everywhere and successfully stops the projectile. The displacements at this point (fig. 10(d)) indicate a definite bulge. The effects of yield strength in general again indicate much greater velocity decreases and much smaller displacements than when the yield strength is neglected.

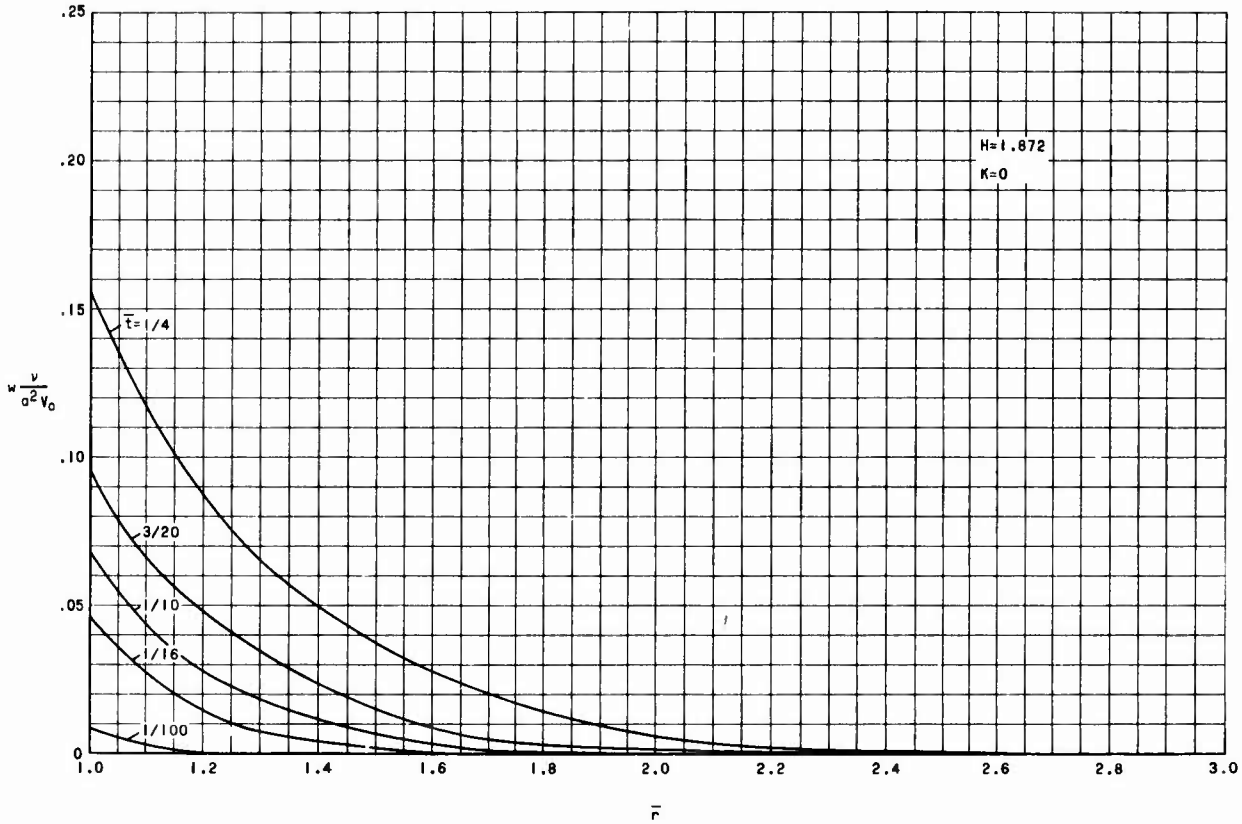

(c) Displacement as a function of radius for $K = 0$.

Figure 10.- Continued.

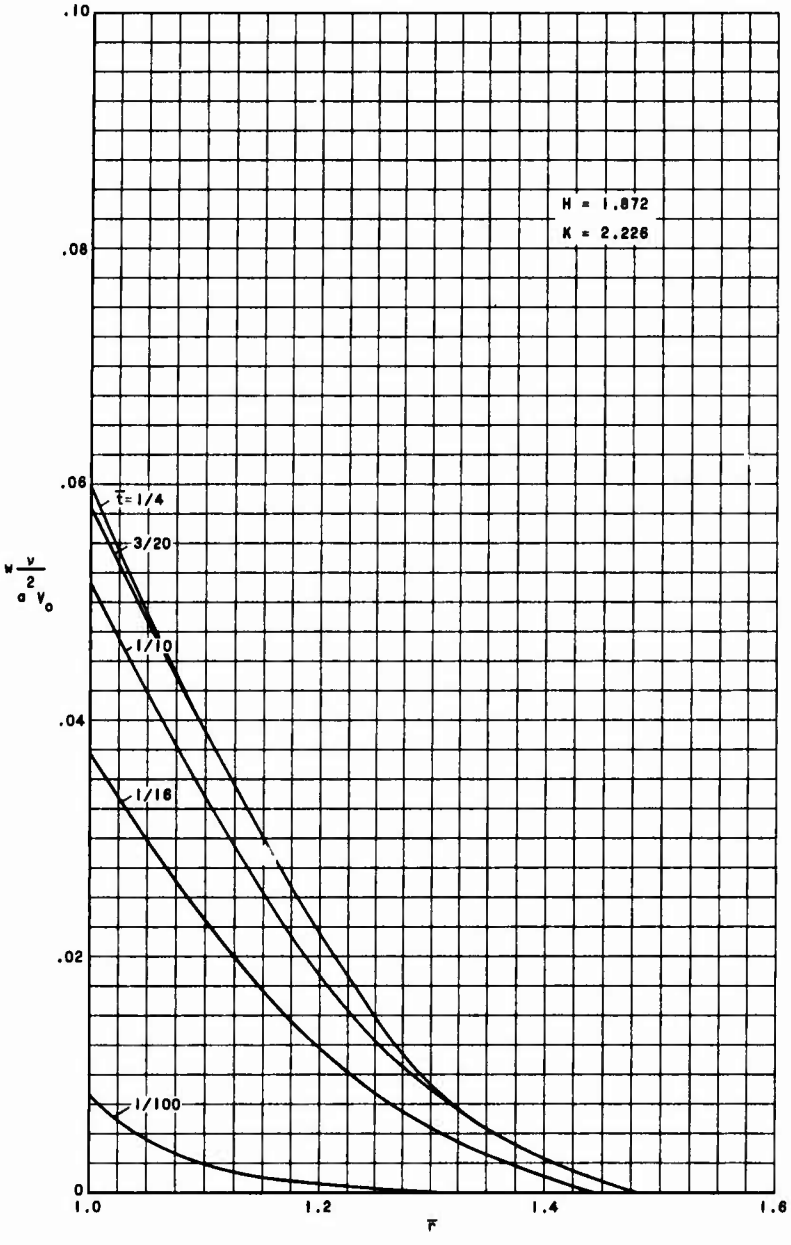

(d) Displacement as a function of radius for K = 2.226.

Figure 10.- Concluded.

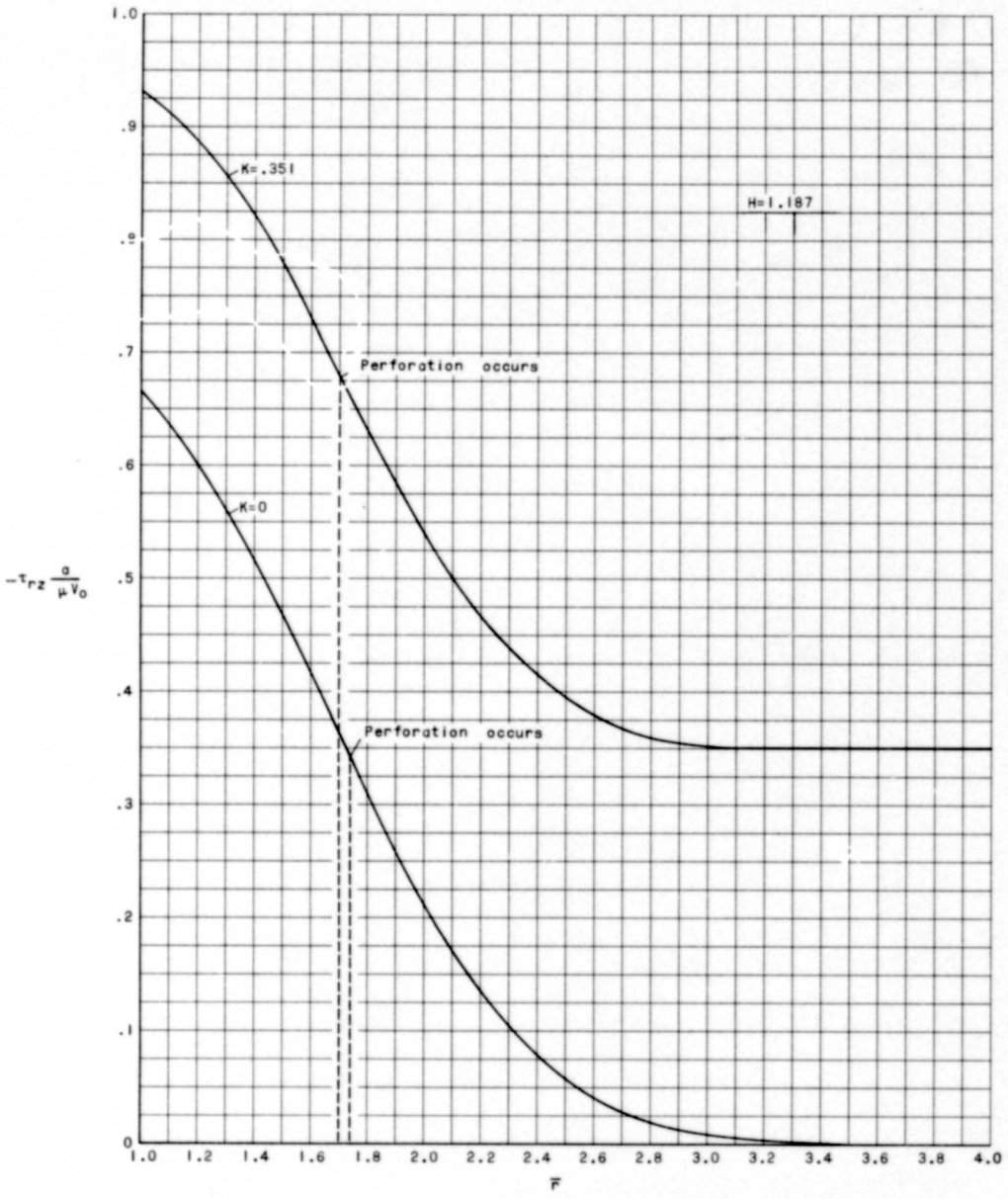

Figure 11.- Shear stress as a function of radius at time of perforation $\bar{t} = 0.25$ for $K = 0$ and $K = 0.351$. $h = 0.25$ inch (0.635 cm); $M_1 = 3.56 \times 10^{-6}$ slug (51.95 mg); $\mu = 100 \frac{\text{slug}}{\text{ft-sec}} \left(0.4788 \frac{\text{Ns}}{\text{cm}^2}\right)$; $g_o = 3{,}940$ fps $\left(1{,}201 \frac{\text{m}}{\text{s}}\right)$; $\rho = 5.2 \frac{\text{slug}}{\text{ft}^3} \left(2.68 \frac{\text{g}}{\text{cm}^3}\right)$; $k = 100{,}000$ psi $\left(68.95 \frac{\text{kN}}{\text{cm}^2}\right)$; $a = 0.04688$ inch (0.119 cm).

Stresses

When the radial distribution of shear stresses present in the plate after impact are computed from the analysis with and without yield strength, it is obvious from equation (2b) that they will differ. In fact, the variance at the time and radius of perforation is approximately 2 to 1. In figure 11 is shown a distribution of shear stress computed at the dimensionless time of $\bar{t} = 0.25$ (calculated separation times are actually $\bar{t} = 0.24$ for $K = 0$ and $\bar{t} = 0.23$ for $K \neq 0$) for a 1/4 inch (0.635 cm) aluminum plate. The initial projectile velocity was taken to be 3,940 fps (1,201 m/s) and the radius of perforation at separation is indicated by the dashed lines in figure 11. As can be seen from figure 11, the shearing stresses occurring at the radius of perforation computed by use of the two different solutions differ by a ratio of about 2 to 1.

CONCLUDING REMARKS

It has been shown in the present paper that the inclusion of target-material yield strength in a one-dimensional analysis of hypervelocity impact perforations has produced little effect on the resulting perforation radii. The variation in calculated perforation radii as compared with the solution neglecting target yield strength amounts to only 5 percent. This percent difference in calculated perforation radii remains at the negligible 5-percent level even with variations in the pertinent parameters such as plate (or target) thickness, projectile mass, and initial velocity. With variations in the dynamic coefficient of viscosity, the difference does increase to perhaps 10 percent but the variations in perforation radius due to differences in the assumed value of the viscosity coefficient alone are much greater than the 10 percent present when yield strength is neglected. In fact, the determination of accurate values for the dynamic coefficient of viscosity is much more critical in the calculation of perforation radii than is the inclusion of the target yield strength.

In the determination of the minimum thickness of plate necessary for prevention of perforation, however, the effect of yield strength may be important depending on the initial velocity and mass of the projectile, and the present analysis containing yield strength should be applied. Furthermore, parametric studies in which not only the initial projectile velocity is varied but also the thickness of the plate and the mass of the projectile could provide pertinent data as to minimum thicknesses of target material needed to prevent perforations.

The velocities, displacements, and stresses can be markedly different in the resulting calculations for hypervelocity impact depending upon whether target yield strength has been included in the analysis or not. The effects of yield strength in general are to produce much greater velocity decreases and much smaller displacements than those obtained when the yield strength is neglected. In fact, for the particular case where the projectiles do not perforate the target plate, the analysis including yield strength indicates that the velocity drops to zero and the plate is deformed, whereas if the yield

strength is neglected, the velocity only approaches a limiting value, which is not zero. Thus, for this particular case, the velocities, displacements, and stresses calculated by using the simplified solution may be grossly in error.

Langley Research Center,
National Aeronautics and Space Administration,
Langley Station, Hampton, Va., September 30, 1964.

APPENDIX

GOVERNING EQUATION OF SHEAR PERFORATION

An analytical solution is presented for the governing linear differential equation and its associated boundary conditions. In a manner similar to that employed by Chou in reference 3, the governing partial differential equation is reduced to a total differential equation by use of Laplace transform techniques. To obtain a particular solution to the resulting total differential equation, a further change in variables becomes necessary. After satisfying the associated boundary conditions, a "short time" solution is determined by employing asymptotic approximations in the transformed state.

The governing linear differential equation of motion in the axial direction, for simple shear perforation, as derived in the text (see eq. (3)) can be written as

$$\frac{\partial^2 V}{\partial r^2} + \frac{1}{r}\frac{\partial V}{\partial r} - \frac{1}{\nu}\frac{\partial V}{\partial t} = \frac{1}{r}\frac{k}{\mu} \tag{A1}$$

Transforming equation (A1) with respect to t by use of Laplace transform techniques results in

$$\frac{d^2\bar{V}}{dr^2} + \frac{1}{r}\frac{d\bar{V}}{dr} - \frac{1}{\nu}\left[s\bar{V} - V(0,r)\right] = \frac{1}{r}\frac{k}{\mu s} \tag{A2}$$

where s is the transform parameter. By use of the initial condition (eq. (4)) $V(0,r) = 0$ at $t = 0$, $r > a$, equation (A2) is reduced to

$$\frac{d^2\bar{V}}{dr^2} + \frac{1}{r}\frac{d\bar{V}}{dr} - \frac{s\bar{V}}{\nu} = \frac{1}{r}\frac{k}{\mu s} \tag{A3}$$

Let

$$r = -\frac{iz}{\sqrt{\frac{s}{\nu}}} \tag{A4}$$

Hence

$$\frac{d\bar{V}}{dr} = \frac{d\bar{V}}{dz}i\sqrt{\frac{s}{\nu}} \tag{A5}$$

$$\frac{d^2\bar{V}}{dr^2} = -\frac{d^2\bar{V}}{dz^2}\frac{s}{\nu} \tag{A6}$$

and by substitution of these relations into equation (A3) there results

$$\frac{d^2\bar{V}}{dz^2} + \frac{1}{z}\frac{d\bar{V}}{dz} + \bar{V} = -\frac{i}{\sqrt{\frac{s}{\nu}}}\frac{k}{\mu s z} \tag{A7}$$

The homogeneous solution for $\bar{V}(z)$ can be written directly as

$$\bar{V}_H(z) = AJ_0(z) + BY_0(z) \tag{A8}$$

For the particular solution to equation (A7) the Struve function of zero order is satisfactory. A known relation for the Struve function of order p is (see ref. 7, p. 211)

$$\frac{d^2S_p(z)}{dz^2} + \frac{1}{z}\frac{dS_p(z)}{dz} + \left(1 - \frac{p^2}{z^2}\right)S_p(z) = \frac{\left(\frac{z}{2}\right)^{p-1}}{\sqrt{\pi}(p - 0.5)!} \tag{A9}$$

Let $p = 0$; then

$$\frac{d^2S_0(z)}{dz^2} + \frac{1}{z}\frac{dS_0(z)}{dz} + S_0(z) = \frac{2}{z\pi} \tag{A10}$$

Hence, the particular solution to equation (A7) for $\bar{V}(z)$ can be written as

$$\bar{V}_p(z) = -\frac{\pi i}{2\sqrt{\frac{s}{\nu}}}\frac{k}{\mu s}S_0(z) \tag{A11}$$

and the general solution becomes

$$\bar{V}(z) = \bar{V}_H(z) + \bar{V}_p(z) = AJ_0(z) + BY_0(z) - \frac{\pi i k}{2\sqrt{\frac{s}{\nu}}\mu s}S_0(z) \tag{A12}$$

or resubstituting for z from equation (A4)

$$\bar{V}(r,s) = AJ_0\left(ir\sqrt{\frac{s}{\nu}}\right) + BY_0\left(ir\sqrt{\frac{s}{\nu}}\right) - \frac{\pi i k}{2\sqrt{\frac{s}{\nu}}\mu s}S_0\left(ir\sqrt{\frac{s}{\nu}}\right) \tag{A13}$$

APPENDIX

In order to apply the (transformed) boundary condition given by equation (8), namely, $\bar{V} = 0$ as $r \to \infty$, one must consider the asymptotic behavior of the solution as given by equation (A13) for $|r| \gg 1$. The asymptotic approximation for the Struve function of order zero as found in equation (136a) of reference 8 is

$$S_0\left(ir\sqrt{\frac{s}{\nu}}\right) \approx Y_0\left(ir\sqrt{\frac{s}{\nu}}\right) + \frac{2}{\pi ir\sqrt{\frac{s}{\nu}}} \tag{A14}$$

and since a known identity between the Bessel functions is (see eq. (110) of ref. 8)

$$K_0\left(r\sqrt{\frac{s}{\nu}}\right) = \frac{\pi}{2}i\left[I_0\left(r\sqrt{\frac{s}{\nu}}\right) + iY_0\left(ir\sqrt{\frac{s}{\nu}}\right)\right] \tag{A15}$$

then

$$S_0\left(ir\sqrt{\frac{s}{\nu}}\right) \approx iI_0\left(r\sqrt{\frac{s}{\nu}}\right) - \frac{2}{\pi}K_0\left(r\sqrt{\frac{s}{\nu}}\right) + \frac{2}{\pi ir\sqrt{\frac{s}{\nu}}} \tag{A16}$$

Hence, for $|r| \gg 1$, the general solution can be written as

$$\bar{V}(r,s) \approx AI_0\left(r\sqrt{\frac{s}{\nu}}\right) + B\left[iI_0\left(r\sqrt{\frac{s}{\nu}}\right) - \frac{2}{\pi}K_0\left(r\sqrt{\frac{s}{\nu}}\right)\right] + \frac{\pi k}{2\sqrt{\frac{s}{\nu}}\mu s}I_0\left(r\sqrt{\frac{s}{\nu}}\right) + \frac{ik}{\sqrt{\frac{s}{\nu}}\mu s}K_0\left(r\sqrt{\frac{s}{\nu}}\right) - \frac{k}{r\frac{s^2}{\nu}\mu} \tag{A17}$$

Application of the transformed boundary condition $\bar{V} = 0$ as $r \to \infty$ (see eq. (8)) yields the relation

$$A = -Bi - \frac{\pi k}{2\sqrt{\frac{s}{\nu}}\mu s} \tag{A18}$$

since $K_0 \to 0$ and $I_0 \to \infty$ as $r \to \infty$. Use of the known identities between $K_0\left(r\sqrt{\frac{s}{\nu}}\right)$ (eq. (A15)), $S_0\left(ir\sqrt{\frac{s}{\nu}}\right)$ (eq. (A14)), $I_0\left(r\sqrt{\frac{s}{\nu}}\right)$, and $Y_0\left(ir\sqrt{\frac{s}{\nu}}\right)$ reduces the general solution to

$$\bar{V}(r,s) = -B\frac{2}{\pi}K_0\left(r\sqrt{\frac{s}{\nu}}\right) - \frac{\pi k}{2\sqrt{\frac{s}{\nu}}\mu s}I_0\left(r\sqrt{\frac{s}{\nu}}\right) - \frac{\pi ik}{2\sqrt{\frac{s}{\nu}}\mu s}S_0\left(ir\sqrt{\frac{s}{\nu}}\right) \tag{A19}$$

APPENDIX

Application of the (transformed) boundary condition (see eq. (7); note also eq. (5))

$$s\bar{V} - \zeta\mu\frac{d\bar{V}}{dr} + \zeta\frac{k}{s} = V_o \qquad (r = a,\ t > 0) \qquad \text{(A20)}$$

permits the evaluation of the quantity B. Substitution of equation (A19) into equation (A20) and use of equation (140a) of reference 8 yield the following expression for B:

$$B = \frac{-V_o - \frac{\pi k}{2\sqrt{\frac{s}{\nu}}\mu} I_0\left(a\sqrt{\frac{s}{\nu}}\right) - S_0\left(ia\sqrt{\frac{s}{\nu}}\right)\frac{\pi i k}{2\mu\sqrt{\frac{s}{\nu}}} + \zeta\frac{\pi k}{2s} I_1\left(a\sqrt{\frac{s}{\nu}}\right) - \zeta\frac{\pi k}{2s}\left[\frac{2}{\pi} - S_1\left(ia\sqrt{\frac{s}{\nu}}\right)\right] + \zeta\frac{k}{s}}{\frac{2}{\pi}\left[sK_0\left(a\sqrt{\frac{s}{\nu}}\right) + \zeta\mu\sqrt{\frac{s}{\nu}}K_1\left(a\sqrt{\frac{s}{\nu}}\right)\right]} \qquad \text{(A21)}$$

Hence, the general solution can be written as

$$\bar{V}(r,s) = \frac{\left\{V_o + \frac{\pi k}{2\sqrt{\frac{s}{\nu}}\mu} I_0\left(a\sqrt{\frac{s}{\nu}}\right) + S_0\left(ia\sqrt{\frac{s}{\nu}}\right)\frac{\pi i k}{2\mu\sqrt{\frac{s}{\nu}}} - \zeta\frac{\pi k}{2s} I_1\left(a\sqrt{\frac{s}{\nu}}\right) + \zeta\frac{\pi k}{2s}\left[\frac{2}{\pi} - S_1\left(ia\sqrt{\frac{s}{\nu}}\right)\right] - \zeta\frac{k}{s}\right\} K_0\left(r\sqrt{\frac{s}{\nu}}\right)}{sK_0\left(a\sqrt{\frac{s}{\nu}}\right) + \zeta\mu\sqrt{\frac{s}{\nu}}K_1\left(a\sqrt{\frac{s}{\nu}}\right)}$$

$$- \frac{\pi k}{2\mu s\sqrt{\frac{s}{\nu}}} I_0\left(r\sqrt{\frac{s}{\nu}}\right) - S_0\left(ir\sqrt{\frac{s}{\nu}}\right)\frac{\pi i k}{2\mu s\sqrt{\frac{s}{\nu}}} \qquad \text{(A22)}$$

A "short time" solution is now determined from the general solution by assuming $a\sqrt{\frac{s}{\nu}} > 1$. By reference again to equation (136a) of reference 8, it can be shown that

$$S_1\left(ia\sqrt{\frac{s}{\nu}}\right) \approx Y_1\left(ia\sqrt{\frac{s}{\nu}}\right) + \frac{2}{\pi} - \frac{2}{\pi a^2\frac{s}{\nu}} \qquad \text{(A23)}$$

A known identity between the modified Bessel function of the second kind of order one K_1 and the Hankel function of the first kind of order one $H_1^{(1)}$ is (see eqs. (115) and (70) of ref. 8)

$$K_1\left(a\sqrt{\frac{s}{\nu}}\right) = -\frac{\pi}{2}H_1^{(1)}\left(ia\sqrt{\frac{s}{\nu}}\right) = -\frac{\pi}{2}\left[J_1\left(ia\sqrt{\frac{s}{\nu}}\right) + iY_1\left(ia\sqrt{\frac{s}{\nu}}\right)\right] \qquad \text{(A24)}$$

Hence

$$J_1\left(ia\sqrt{\frac{s}{\nu}}\right) = -iY_1\left(ia\sqrt{\frac{s}{\nu}}\right) - \frac{2}{\pi}K_1\left(a\sqrt{\frac{s}{\nu}}\right) \tag{A25}$$

and since

$$I_1\left(a\sqrt{\frac{s}{\nu}}\right) = -iJ_1\left(ia\sqrt{\frac{s}{\nu}}\right) \tag{A26}$$

then, from equation (A25)

$$I_1\left(a\sqrt{\frac{s}{\nu}}\right) = -Y_1\left(ia\sqrt{\frac{s}{\nu}}\right) + \frac{2i}{\pi}K_1\left(a\sqrt{\frac{s}{\nu}}\right) \tag{A27}$$

Thus,

$$\frac{2}{\pi} - S_1\left(ia\sqrt{\frac{s}{\nu}}\right) \approx I_1\left(a\sqrt{\frac{s}{\nu}}\right) + \frac{2}{\pi a^2\frac{s}{\nu}} - \frac{2i}{\pi}K_1\left(a\sqrt{\frac{s}{\nu}}\right) \tag{A28}$$

Substitution of the asymptotic expressions for S_0 and $\frac{2}{\pi} - S_1$ into the general solution (eq. (A22)) and making use of the identity for Y_0 (eq. (A15)) yield

$$\bar{V}(r,s) = \frac{\left(V_o + \frac{k}{a\rho s} - \zeta\frac{k}{s} + \zeta\frac{k\nu}{a^2s^2}\right)K_0\left(r\sqrt{\frac{s}{\nu}}\right)}{sK_0\left(a\sqrt{\frac{s}{\nu}}\right) + \zeta\mu\sqrt{\frac{s}{\nu}}K_1\left(a\sqrt{\frac{s}{\nu}}\right)} - \frac{k}{\rho s^2 r} \tag{A29}$$

Note that for increased accuracy in equation (A29), it is only necessary to increase the number of terms taken in the asymptotic expansions of S_0 and S_1; of course, the semiconvergent nature of the asymptotic expansions must be considered. These additional terms are polynomials and would not present any new difficulties. To aid in determining the inverse transform of equation (A29), the following asymptotic expansions of the modified Bessel functions K_0, K_1 are employed (see eq. (114) of ref. 8)

$$\left.\begin{aligned} K_0(z) &= \sqrt{\frac{\pi}{2z}}e^{-z}\left(1 - \frac{1}{8z} + \frac{9}{128z^2} + \cdots\right) \\ K_1(z) &= \sqrt{\frac{\pi}{2z}}e^{-z}\left(1 + \frac{3}{8z} - \frac{15}{128z^2} + \cdots\right) \end{aligned}\right\} \tag{A30}$$

APPENDIX

Substitution of the asymptotic expansions given in equation (A30) into equation (A29) yields after algebraic manipulation:

$$\bar{V}(r,s) = \left(\frac{a}{r}\right)^{\frac{1}{2}} e^{-\sqrt{\frac{s}{\nu}}(r-a)}\left[\frac{V_o}{s} + \frac{1}{s^2}\left(\frac{k}{a\rho} - \zeta k\right) + \frac{1}{s^3}\zeta\frac{k\nu}{a^2}\right]\left[1 - \left(\zeta\frac{\mu}{\nu} + \frac{a-r}{8ra}\right)\frac{1}{\sqrt{\frac{s}{\nu}}}\right.$$

$$\left. + \left(\frac{9a^2 - 2ar - 7r^2}{128a^2r^2} + \zeta\frac{\mu}{\nu}\frac{a-5r}{8ra} + \zeta^2\frac{\mu^2}{\nu^2}\right)\frac{1}{\frac{s}{\nu}} + \cdots\right] - \frac{k}{\rho s^2 r} \qquad \text{(A31)}$$

and by application of standard transform tables (ref. 9, p. 380, formulas (11)) $\bar{V}$ becomes

$$V(r,t) = V_o\left(\frac{a}{r}\right)^{1/2}\left[\operatorname{erfc}\frac{r-a}{2\sqrt{\nu t}} + \left(\frac{r-a}{8r} - \zeta\frac{\mu a}{\nu}\right)\frac{2\sqrt{\nu t}}{a}\,i\operatorname{erfc}\frac{r-a}{2\sqrt{\nu t}}\right.$$

$$\left. + \left(\frac{9a^2 - 2ar - 7r^2}{128r^2} + \zeta\frac{\mu a}{\nu}\frac{a-5r}{8r} + \zeta^2\frac{\mu^2a^2}{\nu^2}\right)\frac{4\nu t}{a^2}i^2\operatorname{erfc}\frac{r-a}{2\sqrt{\nu t}} \cdots\right]$$

$$+ k\left(\frac{1}{\rho a} - \zeta\right)\left(\frac{a}{r}\right)^{1/2}\left[4ti^2\operatorname{erfc}\frac{r-a}{2\sqrt{\nu t}} + \left(\frac{r-a}{8r} - \zeta\frac{\mu a}{\nu}\right)\frac{\sqrt{\nu}}{a}(4t)^{3/2}i^3\operatorname{erfc}\frac{r-a}{2\sqrt{\nu t}}\right.$$

$$\left. + \left(\frac{9a^2 - 2ar - 7r^2}{128r^2} + \zeta\frac{\mu a}{\nu}\frac{a-5r}{8r} + \zeta^2\frac{\mu^2a^2}{\nu^2}\right)\frac{16\nu t^2}{a^2}i^4\operatorname{erfc}\frac{r-a}{2\sqrt{\nu t}} \cdots\right]$$

$$+ \zeta\frac{k\mu}{\rho a^2}\left(\frac{a}{r}\right)^{1/2}\left[16t^2i^4\operatorname{erfc}\frac{r-a}{2\sqrt{\nu t}} + \left(\frac{r-a}{8r} - \zeta\frac{\mu a}{\nu}\right)\frac{\sqrt{\nu}}{a}(4t)^{5/2}i^5\operatorname{erfc}\frac{r-a}{2\sqrt{\nu t}}\right.$$

$$\left. + \left(\frac{9a^2 - 2ar - 7r^2}{128r^2} + \zeta\frac{\mu a}{\nu}\frac{a-5r}{8r} + \zeta^2\frac{\mu^2a^2}{\nu^2}\right)\frac{\nu}{a^2}64t^3i^6\operatorname{erfc}\frac{r-a}{2\sqrt{\nu t}} \cdots\right] - \frac{kt}{\rho r}$$

$$\left((r-a) \geqq 0\right) \qquad \text{(A32)}$$

where the symbol i^n denotes the nth integral of the complementary error function.

Equation (A32) can now be nondimensionalized as follows:

Let

$$\left.\begin{aligned} \bar{r} &= \frac{r}{a} \\ \bar{t} &= \frac{\nu t}{a^2} \\ H &= \zeta\frac{\mu a}{\nu} = \frac{2\pi a^2 h\rho}{M} \\ K &= \frac{ka}{V_o\mu} \end{aligned}\right\} \tag{A33}$$

Hence, the nondimensional velocity can be written as

$$\frac{V}{V_o} = \frac{1}{\sqrt{\bar{r}}}\left\{\operatorname{erfc}\frac{\bar{r}-1}{2\sqrt{\bar{t}}} + 4K(1-H)\bar{t}\,i^2\operatorname{erfc}\frac{\bar{r}-1}{2\sqrt{\bar{t}}} + 16KH\bar{t}^2 i^4\operatorname{erfc}\frac{\bar{r}-1}{2\sqrt{\bar{t}}}\right.$$

$$+ R_1\left[2\sqrt{\bar{t}}\,i\operatorname{erfc}\frac{\bar{r}-1}{2\sqrt{\bar{t}}} + 8K(1-H)\bar{t}^{3/2} i^3\operatorname{erfc}\frac{\bar{r}-1}{2\sqrt{\bar{t}}} + 32KH\bar{t}^{5/2} i^5\operatorname{erfc}\frac{\bar{r}-1}{2\sqrt{\bar{t}}}\right]$$

$$\left. + R_2\left[4\bar{t}\,i^2\operatorname{erfc}\frac{\bar{r}-1}{2\sqrt{\bar{t}}} + 16K(1-H)\bar{t}^2 i^4\operatorname{erfc}\frac{\bar{r}-1}{2\sqrt{\bar{t}}} + 64KH\bar{t}^3 i^6\operatorname{erfc}\frac{\bar{r}-1}{2\sqrt{\bar{t}}}\right]\cdots\right\} - \frac{K\bar{t}}{\bar{r}}$$

$$\left((\bar{r}-1) \geqq 0\right) \tag{A34}$$

where

$$R_1 = \frac{1}{8} - \frac{1}{8\bar{r}} - H$$

$$R_2 = \frac{9}{128\bar{r}^2} - \frac{1}{64\bar{r}} - \frac{7}{128} + H\left(\frac{1}{8\bar{r}} - \frac{5}{8}\right) + H^2$$

By comparison of equations (A31) and (A32), it can be shown that s is related to $1/4t$ and that $a\sqrt{s/\nu} > 1$ implies $\bar{t} < 1/4$. Nevertheless, calculations indicate that the three-term asymptotic series presented in equation (A30) are only approximately 10 to 15 percent in error for $\bar{t} = 1/2$ $\left(\text{and } a\sqrt{s/\nu} = 1/\sqrt{2}\right)$. Therefore, results are presented in this paper for values of $\bar{t}$ as high as $1/2$. Results for $\bar{t} > 1/2$ should be viewed with increasing skepticism. Differentiation of equation (A34) with respect to $\bar{r}$ yields the nondimensional shear strain rate

APPENDIX

$$\frac{\partial V}{\partial r}\frac{a}{V_o} = \frac{1}{\sqrt{\bar{r}}}\left\{-\frac{1}{\sqrt{\pi\bar{t}}}e^{-\frac{(\bar{r}-1)^2}{4\bar{t}}} + R_3\,\mathrm{erfc}\,\frac{\bar{r}-1}{2\sqrt{\bar{t}}} + 2\sqrt{\bar{t}}\left[R_4 - K(1-H)\right]i\,\mathrm{erfc}\,\frac{\bar{r}-1}{2\sqrt{\bar{t}}}\right.$$

$$+ 4\bar{t}\left[R_5 + K(1-H)R_3\right]i^2\mathrm{erfc}\,\frac{\bar{r}-1}{2\sqrt{\bar{t}}} + 8(\bar{t})^{3/2}\left[K(1-H)R_4 - KH\right]i^3\,\mathrm{erfc}\,\frac{\bar{r}-1}{2\sqrt{\bar{t}}}$$

$$+ 16\bar{t}^2\left[KHR_3 + K(1-H)R_5\right]i^4\mathrm{erfc}\,\frac{\bar{r}-1}{2\sqrt{\bar{t}}} + 32(\bar{t})^{5/2}KHR_4i^5\mathrm{erfc}\,\frac{\bar{r}-1}{2\sqrt{\bar{t}}}$$

$$\left. + 64\bar{t}^3KHR_5i^6\mathrm{erfc}\,\frac{\bar{r}-1}{2\sqrt{\bar{t}}} \cdots\right\} + \frac{K\bar{t}}{\bar{r}^2} \qquad \left((\bar{r}-1) \geq 0\right) \qquad (A35)$$

where

$$R_3 = -\frac{3}{8\bar{r}} - \frac{1}{8} + H$$

$$R_4 = \frac{15}{128\bar{r}^2} - \frac{3}{64\bar{r}} + \frac{7}{128} + \frac{H}{8}\left(\frac{3}{\bar{r}} + 5\right) - H^2$$

$$R_5 = -\frac{45}{256\bar{r}^3} + \frac{3}{128\bar{r}^2} + \frac{7}{256\bar{r}} + \frac{H}{16}\left(\frac{5}{\bar{r}} - \frac{3}{\bar{r}^2}\right) - \frac{H^2}{2\bar{r}}$$

By integration of equation (A35) with respect to $\bar{t}$, the nondimensional shear strain is obtained

$$\frac{\partial w}{\partial r}\frac{\nu}{V_o a} = \frac{4\bar{t}}{\sqrt{\bar{r}}}\left\{-\frac{1}{2\sqrt{\bar{t}}}i\,\mathrm{erfc}\,\frac{\bar{r}-1}{2\sqrt{\bar{t}}} + R_3i^2\mathrm{erfc}\,\frac{\bar{r}-1}{2\sqrt{\bar{t}}} + 2\sqrt{\bar{t}}\left[R_4 - K(1-H)\right]i^3\mathrm{erfc}\,\frac{\bar{r}-1}{2\sqrt{\bar{t}}}\right.$$

$$+ 4\bar{t}\left[R_5 + K(1-H)R_3\right]i^4\mathrm{erfc}\,\frac{\bar{r}-1}{2\sqrt{\bar{t}}} + 8(\bar{t})^{3/2}\left[K(1-H)R_4 - KH\right]i^5\mathrm{erfc}\,\frac{\bar{r}-1}{2\sqrt{\bar{t}}}$$

$$+ 16\bar{t}^2\left[KHR_3 + K(1-H)R_5\right]i^6\mathrm{erfc}\,\frac{\bar{r}-1}{2\sqrt{\bar{t}}} + 32(\bar{t})^{5/2}KHR_4i^7\mathrm{erfc}\,\frac{\bar{r}-1}{2\sqrt{\bar{t}}}$$

$$\left. + 64\bar{t}^3KHR_5i^8\mathrm{erfc}\,\frac{\bar{r}-1}{2\sqrt{\bar{t}}} \cdots\right\} + \frac{K\bar{t}^2}{2\bar{r}^2} \qquad \left((\bar{r}-1) \geq 0\right) \qquad (A36)$$

APPENDIX

A second integration with respect to $\bar{r}$ would determine the corresponding displacement. However, a simpler approach is to integrate the nondimensional velocity with respect to $\bar{t}$ to obtain the nondimensional displacement

$$\frac{w}{a^2 V_o} = \frac{4\bar{t}}{\sqrt{\bar{r}}}\left\{ i^2\mathrm{erfc}\,\frac{\bar{r}-1}{2\sqrt{\bar{t}}} + 4K(1-H)\bar{t}\,i^4\mathrm{erfc}\,\frac{\bar{r}-1}{2\sqrt{\bar{t}}} + 16KH\bar{t}^2 i^6\mathrm{erfc}\,\frac{\bar{r}-1}{2\sqrt{\bar{t}}} \right.$$

$$+ R_1\left[2\sqrt{\bar{t}}\,i^3\mathrm{erfc}\,\frac{\bar{r}-1}{2\sqrt{\bar{t}}} + 8K(1-H)(\bar{t})^{3/2} i^5\mathrm{erfc}\,\frac{\bar{r}-1}{2\sqrt{\bar{t}}} + 32KH(\bar{t})^{5/2} i^7\mathrm{erfc}\,\frac{\bar{r}-1}{2\sqrt{\bar{t}}} \right]$$

$$\left. + R_2\left[4\bar{t}\,i^4\mathrm{erfc}\,\frac{\bar{r}-1}{2\sqrt{\bar{t}}} + 16K(1-H)\bar{t}^2 i^6\mathrm{erfc}\,\frac{\bar{r}-1}{2\sqrt{\bar{t}}} + 64KH\bar{t}^3 i^8\mathrm{erfc}\,\frac{\bar{r}-1}{2\sqrt{\bar{t}}} \right] \cdots \right\} - \frac{K\bar{t}^2}{2\bar{r}}$$

$$((\bar{r}-1) \geqq 0) \qquad \text{(A37)}$$

The symbol $i^n\mathrm{erfc}\,x$ represents the repeated nth integrals of the complementary error function $\mathrm{erfc}\,\xi$

$$i^n\mathrm{erfc}\,x = \int_x^\infty i^{n-1}\mathrm{erfc}\,\xi\,d\xi \qquad \text{(A38)}$$

in which

$$i^0\mathrm{erfc}\,x = \mathrm{erfc}\,x$$

$$i^{-1}\mathrm{erfc}\,x = \frac{2}{\sqrt{\pi}} e^{-x^2}$$

and $x(\xi)$ is the argument of the complementary error function. A recurrence relation useful in determining the repeated integrals of the complementary error function is (see refs. 8 and 9)

$$i^n\mathrm{erfc}\,x = \frac{i^{n-2}\mathrm{erfc}\,x - 2x\,i^{n-1}\mathrm{erfc}\,x}{2n} \qquad \text{(A39)}$$

A table of the error function and its derivatives and integrals for values of the argument between 0 and 3.0 is presented in reference 9 from values given in reference 10. A similar table has been included in this paper, with slight extensions, for convenience in computing these expressions. (See table II.) A table of the first 11 repeated integrals of the error function with values of the argument between 0 and 2.80 is also available. (See ref. 11.)

TABLE II.- FIRST EIGHT REPEATED INTEGRALS OF THE COMPLEMENTARY ERROR FUNCTION

x	erf' x	erfc x	i erfc x	i^2erfc x	i^3erfc x	i^4erfc x	i^5erfc x	i^6erfc x	i^7erfc x	i^8erfc x
0.00	1.12837910	1.00000000	0.56418955	0.25000000	0.09403159	0.03125000	0.00940315	0.00260416	0.00067165	0.00016276
.05	1.12556170	.94362802	.51559945	.22301702	.08221629	.02684942	.00795313	.00217117	.00055257	.00013224
.10	1.11715160	.88753708	.46982210	.19839317	.07169057	.02300688	.00670892	.00180542	.00045341	.00010717
.15	1.10327410	.83200403	.42683645	.17598827	.06233999	.01966078	.00564417	.00149729	.00037107	.00008662
.20	1.08413470	.77729741	.38660787	.15566357	.05405707	.01675509	.00473550	.00123840	.00030286	.00006982
.25	1.06001410	.72367361	.34908865	.13728232	.04674124	.01423896	.00396217	.00102148	.00024653	.00005613
.30	1.03126090	.67137324	.31421848	.12071054	.04029869	.01206641	.00330588	.00084024	.00020012	.00004501
.35	.99828371	.62061795	.28192557	.10581751	.03464221	.01019599	.00275050	.00068922	.00016200	.00003598
.40	.96154130	.57160765	.25212759	.09247640	.02969107	.00859044	.00228187	.00056374	.00013077	.00002869
.45	.92153201	.52451828	.22473278	.08056470	.02537075	.00721637	.00188760	.00045979	.00010527	.00002281
.50	.87878258	.47950012	.19964123	.06996473	.02161275	.00604399	.00155687	.00037392	.00008449	.00001808
.55	.83383665	.43667663	.17674618	.06056396	.01835430	.00504677	.00128028	.00030320	.00006762	.00001430
.60	.78724343	.39614391	.15593537	.05225536	.01553815	.00420119	.00104967	.00024513	.00005396	.00001127
.65	.73954676	.35797067	.13709245	.04493762	.01311225	.00348646	.00085798	.00019758	.00004293	.00000886
.70	.69127486	.32219881	.12009827	.03851530	.01102947	.00288425	.00069915	.00015878	.00003406	.00000694
.75	.64293107	.28884366	.10483279	.03289861	.00924747	.00237842	.00056798	.00012720	.00002694	.00000542
.80	.59498579	.25789904	.09117366	.02800529	.00772753	.00195515	.00045992	.00010160	.00002123	.00000422
.85	.54786972	.22933194	.07900272	.02375682	.00643601	.00160194	.00037127	.00008089	.00001669	.00000328
.90	.50196857	.20309179	.06820167	.02008219	.00534228	.00130826	.00029874	.00006421	.00001308	.00000254
.95	.45761925	.17910919	.05865589	.01691575	.00441932	.00106487	.00023960	.00005080	.00001022	.00000196
1.00	.41510750	.15729921	.05025454	.01419753	.00364324	.00086388	.00019154	.00004006	.00000795	.00000150
1.10	.33647960	.11979493	.03646538	.00989277	.00245021	.00056278	.00012120	.00002467	.00000477	.00000088
1.20	.26734435	.08968602	.02604895	.00679213	.00162463	.00036162	.00007567	.00001500	.00000283	.00000051
1.30	.20820799	.06599206	.01831432	.00459370	.00106178	.00022913	.00004660	.00000899	.00000165	.00000029
1.40	.15894171	.04771488	.01267002	.00305970	.00068380	.00014312	.00002830	.00000532	.00000095	.00000016
1.50	.11893029	.03389485	.00862287	.00200656	.00043386	.00008812	.00001695	.00000310	.00000054	.00000009
1.60	.08722906	.02365162	.00577193	.00129535	.00027113	.00005346	.00001000	.00000178	.00000030	.00000005
1.70	.06271104	.01620954	.00379930	.00082297	.00016686	.00003195	.00000582	.00000101	.00000016	.00000002
1.80	.04419172	.01090950	.00245876	.00051449	.00010109	.00001881	.00000333	.00000056	.00000009	.00000001
1.90	.03052474	.00720957	.00156418	.00031641	.00006030	.00001090	.00000188	.00000031	.00000004	.00000000
2.00	.02066699	.00467774	.00097801	.00019142	.00003538	.00000623	.00000104	.00000017	.00000002	.00000000
2.10	.01371565	.00297947	.00060093	.00011388	.00002043	.00000350	.00000057	.00000009	.00000001	.00000000
2.20	.00892216	.00186285	.00036281	.00006662	.00001161	.00000194	.00000030	.00000004	.00000000	.00000000
2.30	.00568902	.00114318	.00021519	.00003831	.00000648	.00000105	.00000016	.00000002	.00000000	.00000000
2.40	.00355565	.00068851	.00012540	.00002164	.00000358	.00000055	.00000009	.00000000	.00000000	-.00000000
2.50	.00217828	.00040695	.00007176	.00001203	.00000193	.00000029	.00000004	.00000000	.00000000	-.00000000
2.60	.00130805	.00023603	.00004034	.00000655	.00000104	.00000014	.00000003	-.00000000	.00000000	-.00000000
2.70	.00076992	.00013433	.00002226	.00000351	.00000054	.00000007	.00000001	-.00000000	.00000000	-.00000000
2.80	.00044421	.00007501	.00001207	.00000184	.00000029	.00000002	.00000001	-.00000000	.00000000	-.00000000
2.90	.00025121	.00004110	.00000641	.00000097	.00000012	.00000002	-.00000000	.00000000	-.00000000	.00000000
3.00	.00013925	.00002209	.00000335	.00000049	.00000006	.00000000	.00000000	.00000000	.00000000	-.00000000

REFERENCES

1. Bakhshiyan, F. A.: Visco-Plastic Flow by Impact of a Cylinder Upon a Plate. Appl. Math. Mech. (Moscow, Leningrad), vol. 12, no. 1, Jan.-Feb. 1948, pp. 47-52.

2. Chou, Pei Chi: Perforation of Plates by High-Speed Projectiles. Vol. 1 of Developments in Mechanics, J. E. Lay and L. E. Malvern, eds., Plenum Press, 1961.

3. Chou, Pei Chi: Visco-Plastic Flow Theory in Hypervelocity Perforation of Plates. Proc. of the Fifth Symposium on Hypervelocity Impact, vol. 1, pt. 1, Apr. 1962, pp. 307-328. (Sponsored by U.S. Navy, U.S. Army, and U.S. Air Force.)

4. Kraus, H.: Two Dimensional Analysis of a Hypervelocity Impact Upon a Visco-Plastic Plate. Proc. of the Sixth Symposium on Hypervelocity Impact, vol. III, Aug. 1963, pp. 13-40. (Sponsored by U.S. Army, U.S. Air Force, and U.S. Navy.)

5. Chou, Pei Chi; Mortimer, Richard W.; and Llorens, Richard E.: A Parametric Study of the Hypervelocity Perforation of Visco-Plastic Plates. DIT Rept. No. 125-3 (Contract No. DA-36-034-ORD-3672 RD), Drexel Inst. Technol., Jan. 1963.

6. Prager, William: Introduction to Mechanics of Continua. Ginn and Co., c.1961.

7. Jahnke, Eugene; and Emde, Fritz: Tables of Functions. Fourth ed., Dover Publ., 1945.

8. McLachlan, N. W.: Bessel Functions for Engineers. Clarendon Press (Oxford), 1934.

9. Carslaw, H. S.; and Jaeger, J. C.: Conduction of Heat in Solids. First ed., The Clarendon Press (Oxford), 1947.

10. Hartree, D. R.: IX.- Some Properties and Applications of the Repeated Integrals of the Error Function. Mem. Proc. Manchester Lit. Phil. Soc., vol. 80, no. 9, 1935-36, pp. 85-102.

11. Kaye, Joseph: A Table of the First Eleven Repeated Integrals of the Error Function. J. Math. Phys., vol. 34, no. 2, July 1955, pp. 119-125.

NASA-Langley, 1965 L-3847